

1 **Morphological Integration and Modularity in the Hyperkinetic Feeding System of Aquatic-** 2 **foraging Snakes**

3 **Running title: Integration in the Kinetic Snake Skull**

4 Daniel Rhoda^{1,2}, P. David Polly³, Christopher Raxworthy¹, Marion Segall^{1*}

5 1. Department of Herpetology, American Museum of Natural History, Central Park West at 79th Street,
6 New York, NY 10024, USA.

7 2. Committee on Evolutionary Biology, University of Chicago, 5801 S Ellis Ave, Chicago, IL 60637, USA

8 3. Earth & Atmospheric Sciences, Biology, and Anthropology, Indiana University, 1001 E. 10th Street,
9 Bloomington, IN 47405.

10 Corresponding author*: Marion Segall, American Museum of Natural History, Department of
11 Herpetology, Central Park West at 79th Street. New York, NY 10024, marion.segall@live.fr

12 **Abstract**

13 The kinetic skull is a key innovation that allowed snakes to capture, manipulate, and
14 swallow prey exclusively using their heads using the coordinated movement of 8 bones. Despite
15 these unique feeding behaviors, patterns of evolutionary integration and modularity within the
16 feeding bones of snakes in a phylogenetic framework have yet to be addressed. Here, we use a
17 dataset of 60 μ CT scanned skulls and high-density geometric morphometric methods to address
18 the origin and patterns of variation and integration in the feeding bones of aquatic-foraging snakes.
19 By comparing alternate superimposition protocols allowing us to analyze the entire kinetic feeding
20 system simultaneously, we find that the feeding bones are highly integrated, driven predominantly
21 by functional selective pressures. The most supported pattern of modularity contains four modules
22 each associated with distinct functional roles: the mandible, the palatopterygoid arch, the maxilla,
23 and the suspensorium. Further, the morphological disparity of each bone is not linked to its
24 magnitude of integration, indicating that integration within the feeding system does not constrain
25 morphological evolution and that adequate biomechanical solutions to a wide range of feeding
26 ecologies and behaviors is readily evolvable within the constraint due to integration in the snake
27 feeding system.

28 **Key words:** Morphological evolution, snakes, skull, morphometrics, functional modularity,
29 Procrustes superimposition

30 **Introduction**

31 Morphological integration and modularity, defined as the covariances between anatomical
32 traits (integration) and their partitioning into semi-autonomously varying modules (modularity),
33 are key concepts in evolutionary biology and are present at some level in all organisms (Olson &
34 Miller 1958; Wagner 2007; Klingenberg 2008). Morphological integration may be advantageous
35 for maintaining functional associations between traits; however, integration is expected to
36 constrain morphological evolution when the direction of selection is not parallel to the line of least
37 evolutionary resistance, defined by the phenotypic covariance matrix (Wagner & Altenberg 1996;
38 Goswami et al. 2014; Felice et al. 2018; Melo et al. 2016). An integrated phenotype may therefore
39 divert a lineage from evolving across an adaptive landscape along a direct path towards an adaptive
40 peak, consequently deflecting evolutionary responses towards less favorable but more probable
41 regions of morphospace. Modularity thus represents a compromise between complete
42 independence between traits, which promotes evolvability but does not maintain functional
43 associations, and complete integration, which constrains morphological evolution in non-viable
44 ways (Wagner & Altenberg 1996; Goswami 2006). Accordingly, comprehension of the
45 morphological evolution of a clade across macroevolutionary timescales necessarily involves a
46 detailed understanding of the clade's patterns of integration, as well as the processes that generate
47 them. In this paper, we examine patterns of morphological integration and modularity in the highly
48 kinetic feeding system of aquatic-foraging snake skulls (Fig. 1). The acquisition of a higher degree
49 of kinesis in the elements of the face and mandible compared to other vertebrates is a key
50 evolutionary innovation (Caldwell, 2019) which allowed snakes to radiate into over 3789 living
51 species (Aug 2019, Uetz et al. 2019) encompassing a broad ecological, dietary, and geographic
52 diversity.

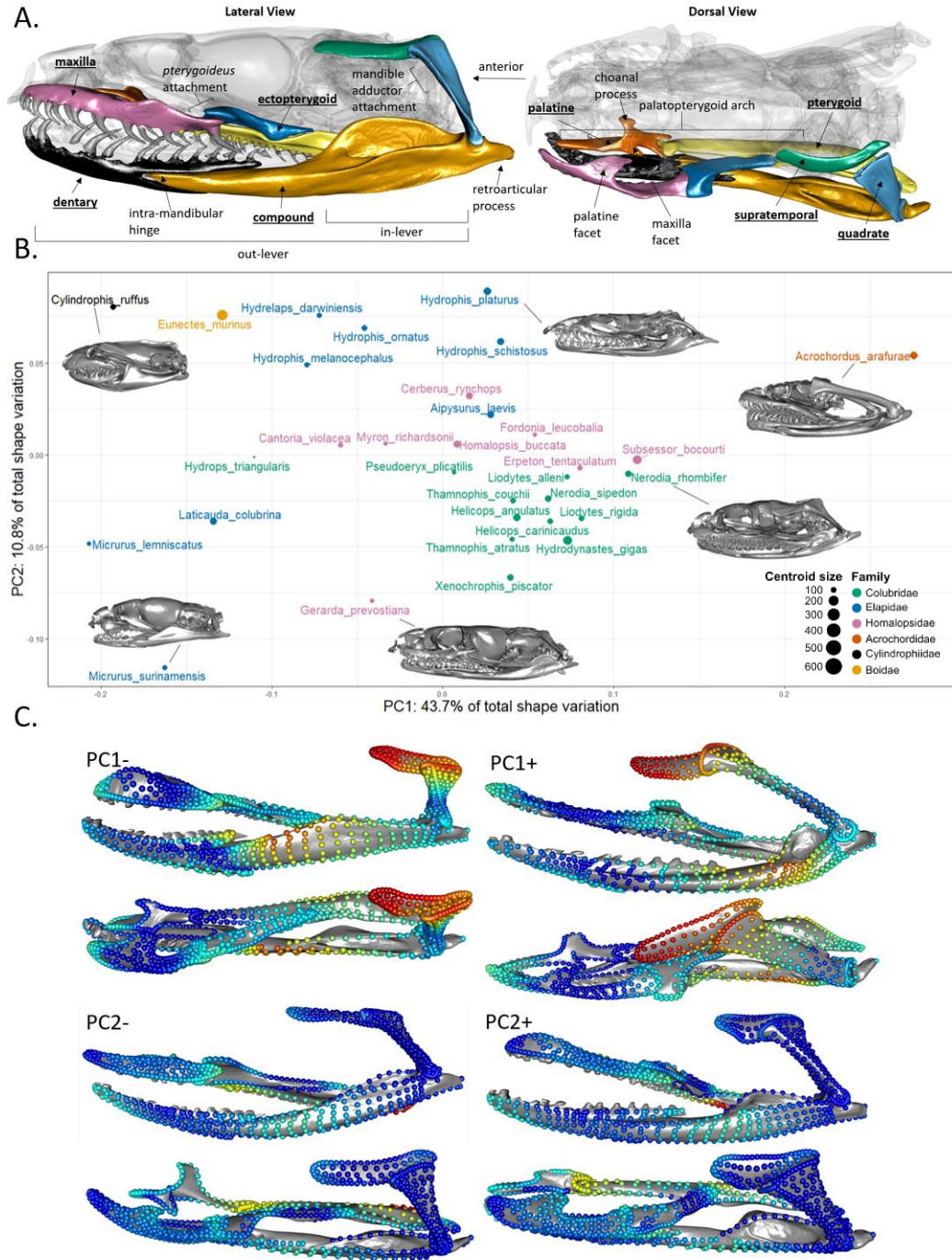
53 The degree and organization of integration among anatomical traits is primarily caused by
54 shared developmental origin and genetic linkages or functional relationships between traits (Olson
55 and Miller 1958; Hallgrímsson et al. 2009). A morphological structure with multiple functions and
56 developmental origins may be both functionally and developmentally modular, not necessarily in
57 overlapping ways (Atchley & Hall 1991; Raff 1996). Disentangling the relative contributions of
58 functional versus development modules will provide a fuller understanding of the
59 macroevolutionary implications of morphological integration because their evolutionary lability
60 reflects the lability and strength of the constraints that populations face in their evolution towards

61 adaptive peaks. For example, if the pattern of evolutionary modularity is caused by a highly
62 conserved suite of developmental pathways, then the macroevolutionary consequences of
63 integration and modularity may be greater than if the same patterns were caused only by functional
64 associations maintained by performance-based selection (Raff 1996). The feeding system of
65 snakes (Fig. 1A) presents an opportunity to study how competing factors translate into patterns of
66 morphological integration and modularity because it is both developmentally and functionally
67 modular in patterns that do not match. If patterns of functional modularity match patterns of
68 evolutionary modularity, then the functional relationships between traits is the primary driver of
69 morphological integration.

70 Snakes are limbless tetrapods that forage almost exclusively using their heads (Cundall and
71 Greene 2000; Moon et al. 2019). The hyperkinetic skulls of snakes are composed of over 20 bones
72 articulated but unfused with one another, 8 of which are directly involved in feeding (Fig. 1A).
73 The extraordinary kinesis of the feeding system facilitates the independent movements of its
74 individual bones which allows exceedingly large gape sizes such that many snakes can ingest prey
75 much larger than they are (Kardong 1977, 1979). The feeding bones are developmentally modular
76 at least insofar that the different bones are ultimately the results of spatially separated developing
77 cellular populations (i.e., the ossification centers of each bone do not meet to fuse together during
78 development, but see Discussion, Raff 1996; Polachowski & Werneburg 2013; Boughner et al.
79 2007). Alternatively, the movements of these spatially separated bones must act in concert to
80 successfully forage; snakes must capture, manipulate, and ingest prey exclusively using their head
81 and anterior trunk (Cundall and Greene 2000; Moon et al. 2019). The feeding sequence of snakes
82 can be divided into several segments: prey capture, prey manipulation and repositioning, and
83 swallowing which includes the highly conserved ‘pterygoid walk’ where the teeth of the palatine
84 and pterygoid grasp and hold onto prey while the braincase advances over it (Bolt and Ewer 1964;
85 Cundall and Greene 2000; Moon et al. 2019). The coordinated movement of different groups of
86 bones are required to perform these different functions, forming functional modules. Bones within
87 a functional module share selective pressures associated with their function and would be expected
88 to covary over evolutionary time. Therefore, in the feeding system of snakes there exists a tension
89 between the kinesis and developmental disintegration of bones promoting modularity and the
90 functional dependencies between those bones promoting integration.

91 Snakes have independently invaded aquatic habits multiple times (over 360 species of snakes
92 use aquatic media, Murphy 2012). The head shape of aquatic foraging snakes has functionally
93 converged in response to the physical constraints related to prey capture under water (Fabre et al.
94 2016; Segall et al. 2016; 2019). Yet, aquatic-foraging snakes show a large amount of
95 morphological variability along with an exceptional ecological diversity in terms of diet, behavior,
96 and habitat-use (Segall et al. 2020), which may be related to the disparate morphology of their
97 feeding bones (Klaczko et al. 2016). The feeding sequence is highly constrained under water, from
98 prey detection, to the hydrodynamic constraints generated by an accelerated strike (Segall 2019;
99 Segall et al. 2020), to the subjugation and manipulation of slippery (e.g. fish, tapdoles), hard (e.g.
100 crustaceans), and elongated preys (e.g. eels), to the lack of constriction in most species, to
101 swallowing a (sometimes living) neutrally-buoyant prey item (Moon et al. 2019). Piscivorous
102 snakes present some specific morphological features in response to these functional constraints
103 such as numerous, longer, sharper teeth (Savitzky 1983). Yet, the morphological and functional
104 relationships between the different bones involved in the feeding sequence remains poorly studied.

105 In the present work, we use high-density 3D geometric morphometrics on the 8 bones that
106 compose the feeding system snakes to explore phylogenetically informed patterns of
107 morphological integration and modularity within a large sample of species that share a functional
108 constraint: aquatic foraging. We investigate morphological integration at all levels: within bones,
109 between bones, and within the whole feeding system. To study morphological integration
110 considering the whole trophic system, we compare two superimposition procedures allowing us to
111 analyze separate mobile (articulating) bones at once, and then directly compare *a priori* hypotheses
112 of modularity using the Covariance Ratio effect size (Adams & Collyer 2019). Focusing on a
113 complex system involving the coordination of several morphologically disparate, developmentally
114 disintegrated bones to fulfil a highly constrained behavior (aquatic foraging), this study aims to
115 understand how functional and developmental modularity is translated into evolutionary
116 integration and modularity, and how these patterns affect morphological disparity over
117 macroevolutionary timescales.



118

119 *Figure 1. (A) The feeding system of snakes (colored) with the anatomical features referenced in this paper*
 120 *labelled on a specimen of Myron richardsonii (AMNH R111792). The labels of bones studied here are*
 121 *underlined>. (B) Scatterplot of the first principal components of a common superimposition of the whole*
 122 *feeding system. Each species is represented as an individual point, the size and color of which corresponds*
 123 *to the centroid size (mm) and taxonomic family (see caption). (C) Shape variation along the first two*
 124 *principal components in lateral (top) and dorsal view (bottom), with landmark colors corresponding to the*
 125 *relative amount that each landmark varies along each PC axis (from PC- to PC+) with red – most variation,*
 126 *and blue – least variation.*

127 **Material and Methods**

128 Sampling and scanning

129 Our taxonomic sampling consisted of 60 adult specimens representing 32 species of aquatic-
130 foraging snakes from a wide taxonomic range (Fig. 1, Supplementary Table 1). Specimens came
131 from multiple Museum collections (AMNH, CAS, FMNH) and were carefully chosen to have the
132 mouth closed with no visible deformation or damage. We performed computed microtomography
133 (CT) scans at a resolution between 15-50 μm , with the Phoenix v|tome| μCT scanner (General
134 Electric Company, Fairfield, CT, USA) at the AMNH Microscopy and Imaging Facility using a
135 voltage between 100-150kV and current between 130-160mA for a voxel size between 15.6-
136 57.4 μm . The 3D reconstruction of the whole skull was performed using the software Phoenix
137 datos|x2 and the subsequent segmentation was done using VGStudioMax v. 3.0 (Volume Graphics
138 GmbH, Heidelberg, Germany). The dentary, compound (here defined as the portion of the
139 mandible posterior to the intramandibular hinge, as in Anjelkovic et al. 2016, 2017), quadrate,
140 supratemporal, pterygoid, ectopterygoid, palatine, and maxilla from the left side of each specimen
141 were digitally separated from the whole skull in GeomagicStudio (3D Systems, Rock Hill). To
142 facilitate the deployment of surface sliding semilandmarks, each bone was cleaned in Geomagic
143 so that small holes were covered, teeth were removed, and surfaces were smoothed following the
144 procedures suggested by Bardua and colleagues (2019a).

145 3D Geometric Morphometrics

146 We used a high-density 3D geometric morphometric approach (1335 total landmarks across
147 all bones) using both anatomical and semilandmarks, to quantify the shapes of each bone (Adams
148 et al. 2004, 2013; Dumont et al. 2016; Goswami et al. 2019). Anatomical landmarks and curve
149 semilandmarks were placed on each bone using IDAV Landmark Editor and MorphoDig
150 (Supplementary Fig. 1; Wiley et al. 2005; Lebrun & Orliac 2017). Using the function ‘placePatch’
151 in the R package *Morpho*, surface landmarks were projected onto each separate bone from a
152 template specimen following the precautions suggested by Bardua and colleagues (2019a;
153 Schlager 2017). Disparity in the shapes of the choanal and maxilla facet of the palatine obstructed
154 the projection of surface landmarks, so the shape of the palatine was represented only with
155 anatomical and curve landmarks. The choanal and maxilla processes were still captured with
156 anatomical and curve landmarks. The curve and surface semilandmarks were allowed to slide to

157 minimize bending energy (Gunz et al. 2005; Gunz & Mitteroecker 2013). We used generalized
158 least-squares Procrustes superimposition with the ‘gpagen’ function in *geomorph* (Rohlf & Slice
159 1990; Adams and Otárola-Castillo 2013) to analyze shape variation in each bone, individually.

160 Shape variability, phylogenetic signal, and allometry

161 To define lines of least resistance, we used principal component analyses (PCA, ‘gm.prcomp’
162 function in *geomorph*) to extract and visualize the main axes of variation for each bone and the
163 whole feeding system (Adams and Otárola-Castillo 2013; see below for an account of how bones
164 were combined to assess the feeding system as a whole). Thin-plate spline deformations applied
165 on meshes were used to visualize the shape variation associated with each axis (‘tps3d’ function
166 in *Morpho*). Using the phylogeny of Pyron and Burbrink (2014) pruned to our dataset
167 (Supplementary Table 1), we tested for a phylogenetic signal in each bone (‘physignal’ function
168 in *geomorph*) to assess whether the phylogenetic relationships between species was related to their
169 morphology (Adams 2014; Adams and Otárola-Castillo 2013). A significant phylogenetic signal
170 was found in each bone ($P < 0.01$, $K < 0.59$, Table 1), so all subsequent analyses were performed in
171 a phylogenetically informed context. To test for the effects of evolutionary allometry on shape, we
172 performed phylogenetic generalized least squares (PGLS) analyses on the Procrustes coordinates
173 and the log-transformed centroid size as a covariate using the ‘procD.pgls’ function in *geomorph*.

174 Modularity analyses and superimposition protocols

175 As employed here, both eigenvalue dispersion and two-block partial least squares measure
176 covariance in shape within and between bones independent of their relative sizes and positions in
177 the mouth (discussed below). However, in the case of the feeding bones of snakes, the relative
178 positions, orientations, and sizes of bones are immensely important to the functional relationships
179 between bones and therefore morphological integration and modularity. For example, a larger gape
180 in many taxa is accomplished by the backwards rotation of the quadrate, such that the quadrate
181 points posteriorly (see *Acrochordus arafurae*, Fig. 1B) rather than orthogonally to the mandible
182 (as in *Cylindrophis ruffus*, Fig. 1B). Further, patterns of ontogenetic allometry in some
183 macrostomatan snakes involve backwards rotation of the quadrate and positive allometry of the
184 jaws, supratemporal length, and quadrate length (Scanferla 2016; Palci et al. 2016), facilitating
185 ontogenetic niche shifts in some species (Vincent et al. 2007; Mushinsky 1982). This allometric
186 axis of shape variation, affecting separate component parts (i.e., potential modules) of the snake

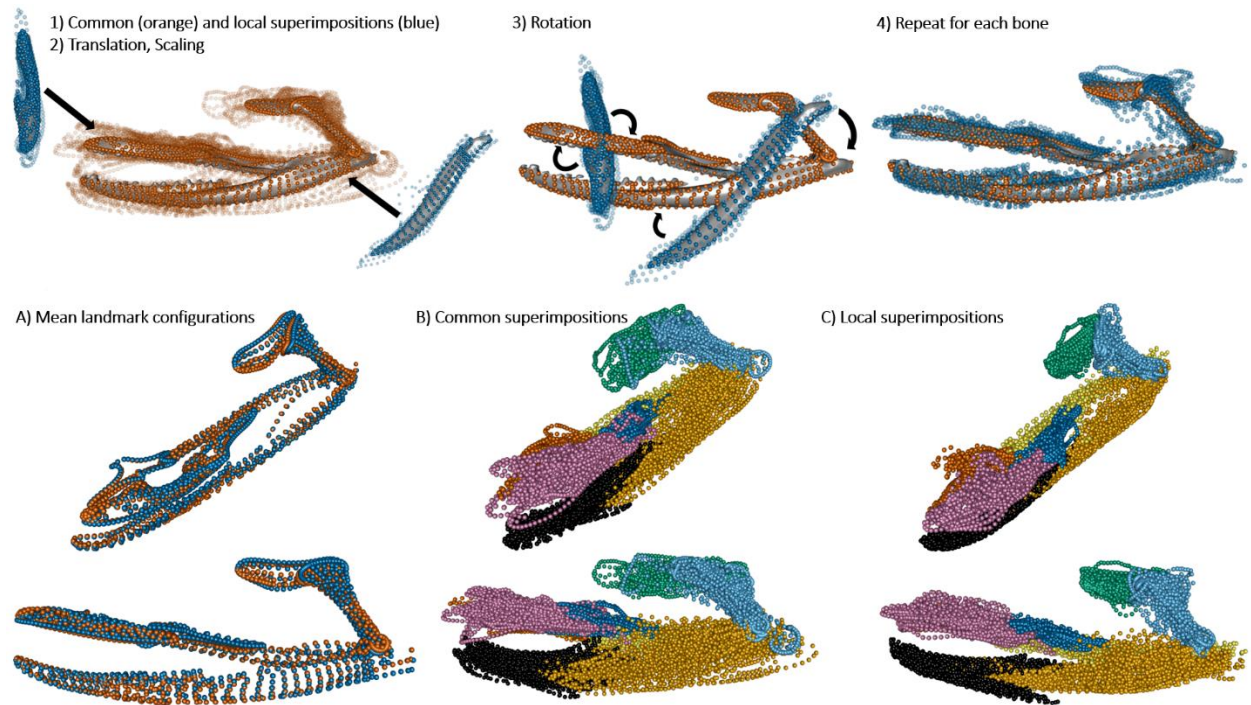
187 feeding system simultaneously, has been demonstrated to be functionally consequential,
188 evolutionary labile, and adaptive (Esquerré et al. 2017, and Sherratt et al. 2019 report heterochronic
189 shifts facilitating dietary shifts), suggesting that it may influence evolutionary integration within
190 the snake skull. A shared coordinate system that maintains the relative sizes and positions of the
191 bones is therefore desirable to understand the patterns of integration and modularity. We employed
192 two superimposition strategies to achieve this goal: a common superimposition and ‘matched’
193 local superimpositions.

194 The common superimposition consisted of performing a GPA on all of the bones at once in
195 their original CT scanned positions, treating them as if they were a single structure (GPA_{all})
196 because in that position the bones all retain their relative sizes and are in a natural resting position
197 relative to one another that is largely repeatable (it is worth noting that no ‘true’ anatomical
198 position exists in a kinetic system, Collyer et al. 2020). Mobility between the bones in a living
199 snake is comparatively small relative to their overall position in this resting orientation (Watanabe
200 et al. 2019, Supplementary Fig. 2). Other authors have adopted a similar strategy for analyzing the
201 shape of the entire feeding apparatus (e.g., Watanabe et al. 2019; Palci et al. 2016; Klaczko et al.
202 2016; Souto et al. 2019; Silva et al. 2018; Murta-Fonseca et al. 2019; dos Santos et al. 2017) and
203 additional studies have superimposed non-rigid structures together in other organisms when taking
204 appropriate precautions (Adams 1999; Rohlf & Corti 2000; Adams & Rohlf 2000; Adams 2004).
205 Each specimen was μ CT scanned with the mouths completely closed; only specimens in neutral
206 poses were included, where articulating bones were positioned directly adjacent to each other.
207 Even though none of the individual bones are fused with one another, numerous soft tissue
208 connections reduce rotational degrees of freedom of each bone. We also corrected for intraspecific
209 variation by averaging landmark configurations per species, which further minimizes the variation
210 due to mobility alone. The position and respective centroid size of each bone in the mean shape
211 (of all species) resulting from this procedure was computed and used in the local superimposition
212 procedure.

213 Because the relative positions of the elements could still vary non-repeatably because of the
214 death position in which the specimen was preserved, we also adopted a second: matched local
215 superimposition. This local superimposition procedure first consisted of performing a GPA for
216 each bone separately. The superimposed landmark coordinates of each bone were then translated,
217 rotated, and scaled to fit its corresponding bone of the mean shape from GPA_{all} (Fig. 2). This

218 procedure allowed us to have a more homologous positioning and respective size for all species
219 and to preserve the intrinsic, pure shape variation of each individual bone. Further, the mean
220 landmark configuration of the common superimposition, for which the local superimpositions
221 were matched onto, was biologically realistic; since each specimen included was in a neutral pose,
222 the landmark configurations average to a shape reflects a specimen in a neutral pose (Fig. 2), and
223 specimens are scattered around the origin of the PC morphospace suggesting that the mean
224 configuration is natural and plausible (Fig. 1B). The interspecific positional and rotational
225 variation between species may be large enough that it confounds interspecific patterns of pure
226 shape variation within bones. The functional and developmental processes that govern the
227 positional variation in bones may not be the same exact processes that govern shape variation in
228 individual bones, and therefore support for alternative patterns of modularity may
229 disproportionately reflect processes that control the positional variation in bones when only
230 considering a common superimposition. The local superimposition procedure set landmark
231 coordinate configurations in a coordinate space that was biologically realistic and reduced the
232 positional and rotational variation due to mobility so that we could analyze patterns of modularity
233 in the whole system while only considering pure shape (co)variation within the feeding system.

234 The two superimposition procedures are complementary: the local superimpositions account
235 for pure shape variation in each bone and the common superimposition emphasizes (co)variation
236 related to the overall configuration of the feeding apparatus. By comparing results from the two
237 procedures, we bracket the ‘true’ pattern of morphological, evolutionary modularity. If both
238 superimposition procedures support similar hypotheses of modularity, then it is unlikely that the
239 pattern arises because of arbitrary differences due to positioning of the mobile elements.



240

241 *Figure 2. Workflow of the local superimposition procedure: 1) Procrustes superimpositions of the whole*
242 *feeding system (i.e. common superimposition; GPA_{all} , orange), and of each individual bone (i.e. local*
243 *superimpositions; blue) are performed. The transparent landmarks are individual species after their*
244 *respective superimpositions. 2) Each local superimposition dataset is translated and scaled to the mean*
245 *centroid size and position of its corresponding bone in the global mean shape from GPA_{all} and (3) rotated.*
246 *4) Final dataset for the local superimposed procedure. (Below) A) Superimposition of the mean*
247 *configurations of the common (orange) and local superimpositions dataset (blue). Complete landmark*
248 *datasets for the common (B) and local (C) superimpositions procedures (color code matches Fig. 1).*

249 Morphological integration and modularity analyses

250 We used three methods to analyze the pattern of morphological integration and modularity.
251 Relative eigenvalue standard deviation (eigenvalue dispersion) was employed to measure the
252 overall degree of morphological integration within each bone and then the feeding system as a
253 whole (Pavlicev et al. 2009). Phylogenetic two-block partial least squares (2BPLS,
254 ‘*phylo.integration*’ function in *geomorph*) analyses were used to assess morphological integration
255 between each pair of bones (Rohlf & Corti 2000; Adams & Felice 2014; Adams & Collyer 2016).
256 The Covariance Ratio was used to test *a priori* hypotheses of modularity based on the whole
257 feeding system (Adams 2016, Adams & Collyer 2019).

258 Eigenvalue dispersion was calculated from a singular value decomposition of the covariance
259 matrix of the Procrustes-superimposed landmark configurations for each bone. Higher eigenvalue
260 dispersion values correspond to larger degrees of morphological integration because a smaller

261 number of eigenvectors will explain a larger portion of total correlated shape variation in more-
262 integrated structures (Pavlicev et al. 2009; Goswami & Polly 2010a). Eigenvalue dispersion values
263 range between 0 and 1 and are comparable across datasets (e.g., different bones, Pavlicev et al.
264 2009).

265 The degree and significance of morphological integration between each pair of bones was
266 quantified using phylogenetic 2BPLS and its effect size (Rohlf & Corti 2000; Adams & Felice
267 2014; Adams & Collyer 2016). For each pair of significantly integrated pairs of bones (p-value <
268 0.05) we describe shape variation along the primary axis of covariation (PLS1) to determine which
269 anatomical structures contribute to covariation (Fig. 4). To test if the magnitude of integration
270 constrains morphological diversity, we conducted two least-squares linear regression analyses
271 with Procrustes variance values (i.e., morphological disparity) against 1) eigenvalue dispersion
272 values (i.e., within-bone integration) and 2) the average 2BPLS effect size for each bone (i.e.,
273 between-bone integration) (Fig. 3).

274 For both superimposition methods, 21 *a priori* hypotheses of modularity were tested using the
275 CR (Adams 2016; Adams & Collyer 2019). Each hypothesis of modularity was based on
276 combinations of associations of bones that would be expected to covary in certain functional or
277 developmental contexts (Supplementary Table 2).

278 To visualize the major axes of correlated shape variation within each module of the most
279 supported hypothesis, we performed phylogenetic PCAs (pPCA, Revell 2009, Adams & Collyer
280 2018) on each module ('gm.prcomp' in *geomorph* with the 'Transform' and 'GLS' parameters set
281 to 'True'). Bones within each module were superimposed together. These per-module
282 superimpositions weren't used for any statistical analysis and were only used for visualization
283 purposes. Shape variation along pPC1 was visualized because it is the axis of most correlated shape
284 variation within each module while accounting for phylogenetic non-independence.

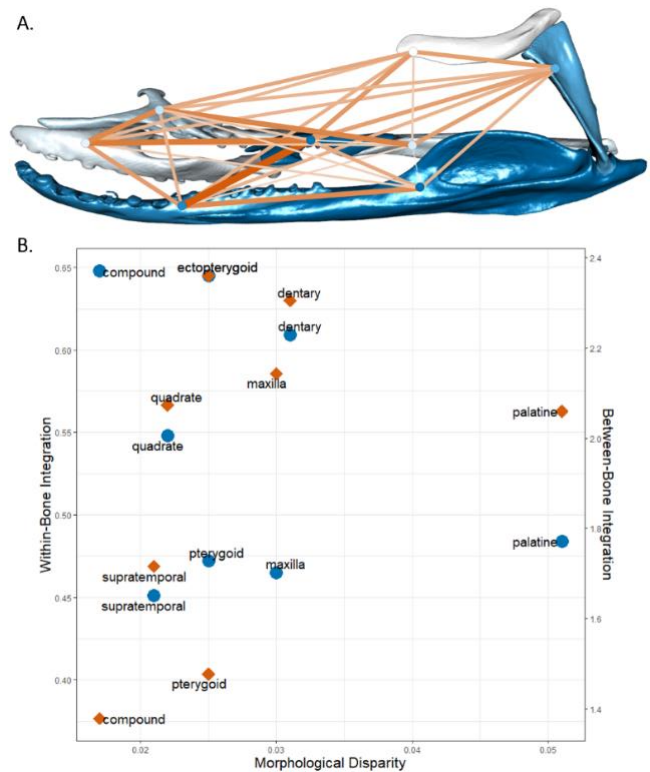
285 **Results**

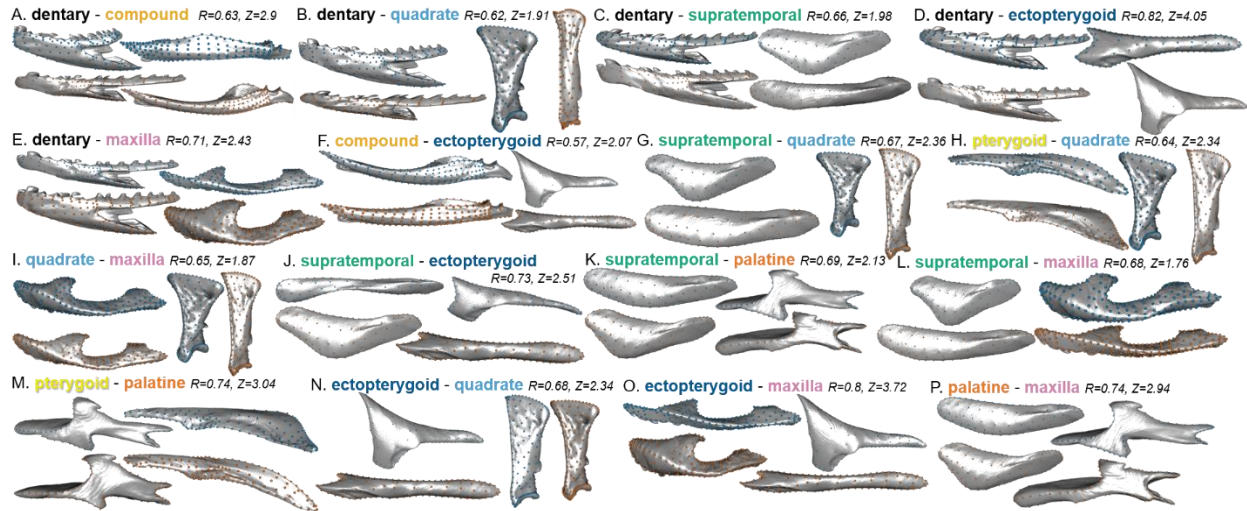
286 Shape variation and covariation of individual bones

287 Significant allometries were found in the quadrate, supratemporal, palatine, and maxilla
288 but explained only a small portion of the shape variation ($R^2=0.6-0.8$) except for the quadrate
289 ($R^2=0.26$, Supplementary Table 3). There was no significant allometry in the dentary, compound,
290 pterygoid and ectopterygoid. The largest eigenvalue dispersions (i.e. within bone integration) were
291 reported in the compound (0.648) and ectopterygoid (0.645) and the smallest in the supratemporal

292 (0.451) and maxilla (0.465) (Supplementary Table 3, Fig. 3). Linear regression analysis showed
293 that the degree of morphological integration within each bone did not significantly relate to
294 morphological disparity (p-value=0.44, Fig. 3). Our 2BPLS analyses recovered significant
295 integration between 16 out of 28 possible pairs of bones (Supplementary Table 4, 5, Fig. 4). The
296 pterygoid is only significantly integrated with the quadrate and palatine, and the compound is only
297 significantly integrated with the dentary and ectopterygoid. The palatine is also integrated with
298 less bones (3) than any of the other bones (each is integrated with 5 other bones) (Fig. 4,
299 Supplementary Table 3, 4). The more strongly integrated pairs are ectopterygoid/dentary (r-
300 PLS=0.822, Fig. 4D) and the ectopterygoid/maxilla (r-PLS=0.806, Fig. 4O). Descriptions of shape
301 variation along PLS1 are provided in the Discussion and shown in Fig. 3. The average 2BPLS
302 effect size for each bone did not significantly relate to morphological disparity (linear regression
303 analysis, p-value=0.173, Fig. 3b).

304 *Figure 3. A) Network graph of within and*
305 *between-bone integration in the feeding*
306 *apparatus. Within-bone integration (eigenvalue*
307 *dispersion values) is represented by the bone*
308 *color: the darker, the stronger. Covariation*
309 *between bones (2BPLS effect size; z-PLS) is*
310 *represented by the color and width of the line*
311 *connecting each pair of bones: wider and darker*
312 *connections correspond to higher effect sizes*
313 *and stronger morphological integration between*
314 *the bones (values in Table 1, Supplementary*
315 *Tables 3-4). B) Scatter plots of morphological*
316 *disparity (x-axis) with within-bone integration*
317 *(eigenvalue dispersion, blue points, left y-axis)*
318 *and between-bone integration (average all the z-*
319 *PLS for each bone, orange points, right y-axis).*
320 *Both regression analyses were not significant.*





321
 322 *Figure 4. Figure 4. Pairwise shape covariation in snake feeding bones along PLS1 from each significant*
 323 *phylogenetic 2B-PLS. (blue: PLS1-; orange: PLS1+)*

324 *Shape variation of the whole feeding apparatus*

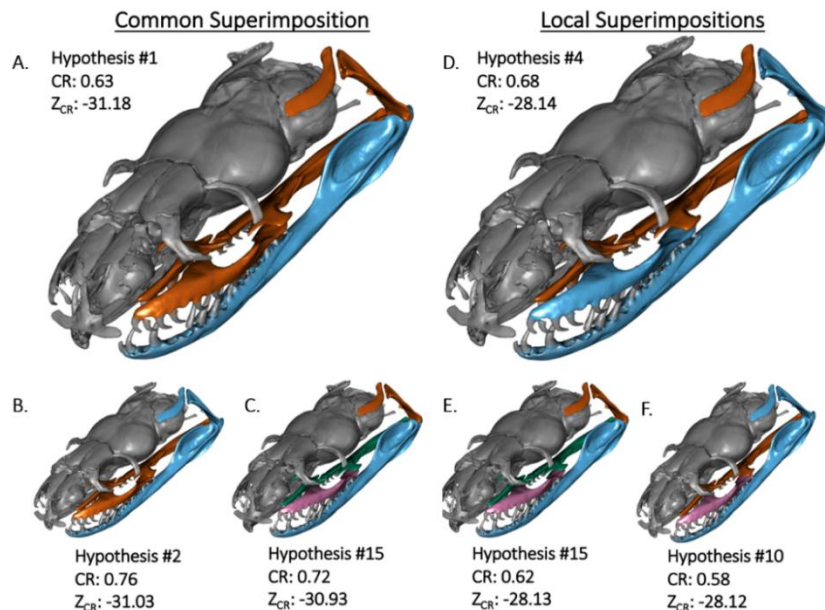
325 Significant allometry was recovered for both the common and local superimposition
 326 datasets containing all bones (p-value=0.001, $R^2=0.13$ and p-value=0.018, $R^2=0.07$, respectively).
 327 The common superimposition showed a larger eigenvalue dispersion value (0.447) than the local
 328 superimposition dataset (0.352).

329 The first principal component (PC1) of the common superimposition dataset (Fig. 1B, C)
 330 accounts for 43.7% of the overall shape variation in the feeding apparatus of snakes and is mainly
 331 driven by the orientation and length of the quadrate, as well as slenderness of the mandible and
 332 maxilla. Shapes at the positive extreme of PC1 (PC1+) had a longer and backwards-rotated
 333 quadrate, and elongated, slender mandibles and maxillas. A ventrally bowed mandible and
 334 prominent palatine processes were characteristic of shapes at PC2-. Colubridae grouped together
 335 except *Hydrops triangularis* (Colubridae) which was separated along PC1, and Homalopsidae are
 336 grouped along PC2, except the crab-tearing specialist *Gerarda prevostiana* (Homalopsidae, Jayne
 337 et al. 2002; Jayne et al. 2018). The elapids showed substantial variation along both PC axes and
 338 drive the variation of PC2, with the true sea snakes (Hydrophiinae) grouping at PC2+ and the semi-
 339 aquatic coral snakes (Micrurinae) at PC2-. *Acrochordus arafurae*'s exceptionally elongated
 340 mandible and quadrate drive the variation along PC1+, while species on PC1- have a short and
 341 almost horizontally positioned quadrate and a dorsally expended prearticular process. Shape
 342 variation along PC2 is smaller, and mainly carried by variation in the palatine-pterygoid joint.

343 Species at PC2- have a dorso-lateral expansion of the posterior part of the pterygoid and a simple
344 shape of the palate-ptyergoid articulation while species at PC2+ have a slender pterygoid with a
345 complex articulation shape.

346 Modularity in the whole feeding apparatus

347 The most supported hypothesis (i.e., the most negative Z_{CR} value, meaning the strongest
348 modular signal) for both common and local superimpositions datasets described two modules (Fig.
349 5). The most supported hypothesis from the common superimposition (H1) described dorso-
350 ventral modularity with mandibular (dentary, compound) and non-mandibular elements as
351 separate evolutionary modules. The most supported hypothesis from the local superimposition
352 dataset (H4) was also composed of two modules, one with the dentary, compound, maxilla and
353 quadrate and the other with the supratemporal, ectopterygoid, pterygoid, palatine, describing a
354 latero-medial pattern modularity. Hypothesis 15 (H15, Fig. 6, Supplementary Table 2, 5) was the
355 third and second most supported hypothesis in the common and local superimposition dataset
356 respectively (Fig. 5). H15 described 4 modules: the mandible, a module with the pterygoid,
357 palatine, and ectopterygoid, the quadrate and supratemporal as a module, and the maxilla as an
358 independent module. Complex hypotheses of modularity (i.e., complete modularity, H21) were
359 not as strongly supported as hypotheses with four or less modules (Supplementary Table 5).

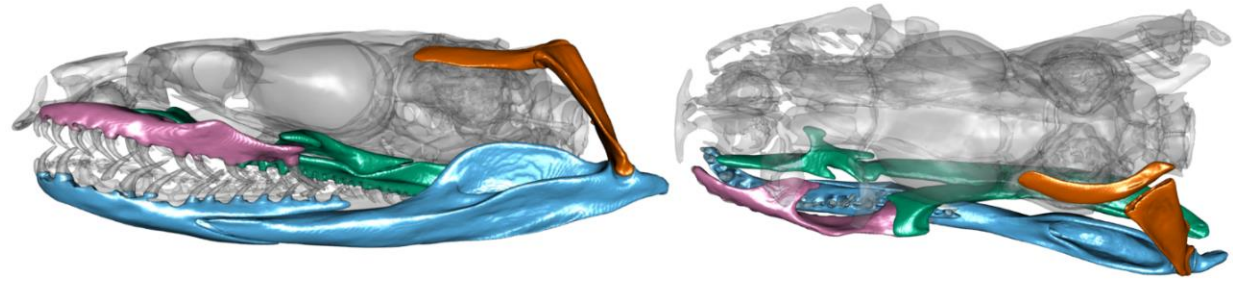


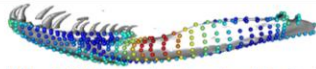
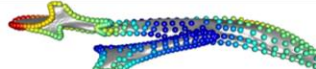
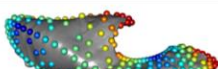
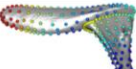
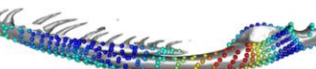
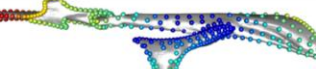


360 *Figure 5. The three most supported hypotheses of snake feeding bone modularity for each superimposition*
361 *method. A, D – most supported hypothesis, B, E – second most supported, C, F – third most supported.*
362 *Each group of similarly colored bones describes a module. The lower the effect size (Z_{CR}), the stronger the*
363 *modular signal, and the more supported the alternative hypothesis. The order of most support is supported*

364 *by pairwise effect size p-values (Supplementary Fig. 11, 12). Note that hypothesis #15 (with four modules)*
365 *is the only hypothesis supported strongly by both superimposition methods.*

366 **Discussion**

367 In the present work, we quantified and compared morphological variability of eight bones
368 that work jointly to fulfill a fitness relevant function (i.e. feeding), at different levels of
369 organization, from covariation within individual bones to patterns of integration and modularity
370 considering all bones, in a phylogenetically informed context. Our results suggest that the feeding
371 apparatus of snakes is highly integrated, predominantly driven by functional relationships between
372 the bones. Our most supported hypotheses describe the mandible and the palatopterygoid arch (i.e.
373 palatine, pterygoid) as two separate modules, with the maxilla and quadrate either integrated with
374 the cranial elements (common superimposition) or the mandibular elements (local
375 superimpositions). The hypothesis with the strongest support from both datasets, H15, contains an
376 integrated palatopterygoid arch (including the ectopterygoid), the maxilla as an independent
377 module, the quadrate and supratemporal as a module, and the mandible as a module. This
378 considerable degree of integration is interesting considering the extreme kinesis of the feeding
379 system, a factor we would generally expect to promote modularity because the bones are not
380 physically coupled with one another and have the freedom to move (and evolve) independently.
381 The high degree of integration within the feeding system supports functional relationships between
382 bones as the primary driver of integration, as the synchronized movements of different
383 combinations of trophic bones is necessary for successful foraging (further discussed below,
384 Cundall and Greene 2000; Moon et al. 2019). These findings also corroborate a recent study by
385 Watanabe and colleagues (2019) who found that the crania of snakes are highly modular, except
386 for the palatopterygoid arch. Although only four bones overlap between their study and ours (the
387 distal quadrate ‘jaw joint’, maxilla, pterygoid, and palatine), we report generally consistent
388 patterns of modularity in the most supported hypotheses (Fig. 5, 6), with an integrated
389 palatopterygoid arch separated from the maxilla and quadrate. Although the maxilla and quadrate
390 are a part of the same module in our most supported hypotheses, they show a moderately low
391 degree of integration, and are a part of separate modules in many other highly supported
392 hypotheses, as is discussed below. Moreover, Watanabe and colleagues (2019) speculated that
393 cranial kinesis may promote integration; we find exceptionally strong integration when
394 considering the most mobile elements of the hyperkinetic snake skull.



Module	Mandible	Palatopterygoid arch	Maxilla	Suspensorium
Function	Prey capture and restraint	Swallowing, pterygoid walk	Prey capture, venom delivery	Gape size
pPC1 -	 MA = 0.39, force advantage, hard-bodied and bulky prey types	 Relative tooth row length = 0.71	 Support for maxillary fangs	 Smaller gape
pPC1 +	 MA = 0.18, speed advantage, elusive prey	 Relative tooth row length = 0.82, slippery prey	 Weaker bite force, more teeth, slippery/elusive prey	 Larger quadrate, backwards rotation

395

396 *Figure 6. A four-module hypothesis (H15) where each module is associated with a distinct functional*
 397 *selective pressure is strongly supported by both superimposition procedures. (Above) Snake skull with the*
 398 *different modules highlighted in different colors in lateral (left) and dorsal (right) view. (Bottom) Per-*
 399 *module shape variation and their functional consequences along phylogenetic PC1. Relative tooth row*
 400 *length was calculated as (length of palatine tooth row + length of pterygoid tooth row) / total anterior-*
 401 *posterior length of the palatopterygoid arch. The color of landmarks represents the magnitude of its*
 402 *variation along pPC1 with red dots varying the most.*

403 Functional and morphological integration in the feeding system

404 Our most supported hypotheses of modularity are consistent with a pattern that arises from
 405 functional aspects of feeding. Prey ingestion is accomplished in most advanced snakes via the
 406 ‘pterygoid walk’, involving the coordinated movement of the palatine and pterygoid bones
 407 (palatopterygoid arch) (Bolt and Ewer 1964; Cundall 1983), accordingly, there are shared
 408 functional selective pressures between these bones. During the pterygoid walk, the palatopterygoid
 409 arch teeth grasp prey while the braincase advances over it. This function is crucial for foraging in
 410 snakes and its performance is especially fitness-related in macrostomatan taxa that ingest large
 411 prey, as snakes are vulnerable to predators during the pterygoid walk (Cundall and Greene 2000).
 412 In aquatic-foraging snakes, selective pressures associated with swallowing may be exacerbated
 413 due to the lubriciousness of prey, or the fact that there may not be a substrate to anchor onto during
 414 the pterygoid walk. The palatine and pterygoid were integrated in our 11 most supported
 415 hypotheses from the common superimposition, and 8 most supported from the local
 416 superimposition dataset. In fact, the hypothesis of complete modularity besides the palatopterygoid

417 arch (H19) was much more supported in both datasets than the hypothesis of complete integration
418 besides the palatopterygoid arch, indicating that the palatopterygoid arch contributes substantially
419 to covariance patterns when considering the whole feeding apparatus. According to 2BPLS
420 analyses neither the palatine nor pterygoid are integrated with more than three different bones.
421 Andjelkovic and colleagues (2017), who also found low integration between the pterygoid and
422 other bones, hypothesized that the pterygoid's functional optimization prevents it from covarying
423 with other bones. Considering the pterygoid's integral role in prey ingestion (hence the 'pterygoid
424 walk') and its physical entanglement with multiple other bones either through articulations or
425 muscle attachments, functional optimization may explain the pterygoid's high integration when
426 considering the whole trophic system but not in 2BPLS analyses. The pterygoid and palatine are
427 also the first bones in the feeding system to ossify (Sheverdyukova 2018; Khannoon & Evans
428 2015; Polachowski & Werneburg 2013; Werneburg et al. 2015), which may promote integration
429 between them (and disintegration between the palatopterygoid arch and the rest of the system)
430 either because of additional, shared opportunity for bone remodeling during development, or a
431 shared influence of morphogens expressed during the palatopterygoid arch's early ossification that
432 the other bones do not face.

433 Strong functional selective pressures drive integration within the mandible as well. The
434 mandible, particularly the compound bone, is directly involved in multiple functional modules.
435 The jaw adductor, responsible for closing the lower jaw and necessary for prey capture, originates
436 on the anteroproximal quadrate and inserts on the mandibular fossa of the compound (Johnston
437 2014). The *pterygoideus*, which moves the palatopterygoid arch ventromedially and the dentary
438 row dorsolaterally during prey ingestion, attaches on the retroarticular compound process and
439 either the ectopterygoid or maxilla (Cundall 1983; Jackson 2003; Johnston 2014, Fig. 1A).
440 Therefore, we would expect the compound to be integrated with the dentary, quadrate,
441 ectopterygoid, and maxilla if functionally relevant muscles solely cause morphological integration.
442 Yet 2BPLS results reveal there is significant integration only with the dentary and ectopterygoid.
443 The PC morphospace and 2BPLS results both suggest that selection for mechanical advantage
444 (MA) is the primary driver of integration within the mandible. The main component of variation
445 in the compound bone (PC1), that accounts for almost 65% of the variation, describes the ratio of
446 the in-lever to the out-lever (Fig. 1A). PC1 of the dentary describes variation in its slenderness and
447 relative length (Supplementary Fig. 3). Shape variation along PLS1 of the dentary and compound

448 mirror this shape variation (Fig. 4a). Taken together, the main axes of variation (PC1) and
449 covariation (PLS1) in the dentary and compound cumulatively describe variation in the MA of the
450 species. Species with a low MA (a longer out-lever compared to in-lever) have a speed advantage
451 and are adapted for capturing elusive prey, and species with a high MA will have a force advantage
452 and are adapted for capturing hard-bodied or bulkier prey (Hampton 2011; Wainwright and
453 Richard 1995; Mori and Vincent 2008). Selection for MA almost certainly promotes integration
454 between the dentary and compound because both separate bones contribute to MA. Further, jaw
455 MA has been related to dietary niche (Mori and Vincent 2008; Hampton 2011), meaning that
456 selection for dietary specializations may promote integration within the mandible. The dentary and
457 compound were significantly integrated (2BPLS) and were a part of the same module in our four
458 most supported hypotheses of modularity (Table 4). This substantial integration within the
459 mandible is functionally relevant, and is particularly interesting considering the evolution of the
460 intra-mandibular hinge that can be considered a form of developmental disintegration in that
461 ossification centers of the dentary and compound do not fuse, a process we would expect to
462 promote modularity, especially if inhibitory signaling obstructs fusion of the ossification centers
463 (Raff 1996). The anatomical liberation between component parts of the mandible is functionally
464 adaptive, as it allows greater mobility and a larger gape (Kardong 1977); in the mandible we find
465 strong morphological integration directly from developmental disintegration.

466 Dietary niche and modularity

467 If the relative importance of different functional modules relates to dietary niche, then it is
468 reasonable to assume that patterns of modularity are influenced by the selective pressures
469 associated with both prey properties and feeding behaviors. For example, eels require different
470 manipulation skills than crabs, however capturing and restraining hard-bodied crabs may require
471 a stronger bite force than required to capture an eel. Consequently, an eel specialist may exhibit a
472 covariance structure such that features associated with prey manipulation are more strongly
473 integrated than features unique to prey capture, and vice versa in a crab-specialist taxon.

474 The *retractor pterygoideus* which originates on the braincase and inserts on the medial palatine
475 along the choanal process, is responsible for advancing the braincase over the prey during the
476 pterygoid walk. The shape of the choanal process on the palatine (C8, C9, Supplementary Fig. 1),
477 is highly variable along PC2 of the common superimposition, and both PC axes of the palatine
478 morphospace (Supplementary Fig. 9). The venomous, pelagic *Hydrophis platurus* completely

479 lacks a choanal process but contains an elongated retroarticular process, providing substantial area
480 for attachment of the *pterygoideus* muscle. Stimulation of the *pterygoideus* muscle induces
481 outward rotation of the dentary tooth row (Cundall 1983). The primary role of the mandible in
482 many taxa during ingestion is to keep prey pressed onto the teeth of the palatopterygoid arch. In a
483 venomous₅₇ pelagic sea snake adapted for elusive and neutrally buoyant prey, selective pressures
484 for prey ingestion may be stronger on morphological features relevant to prey manipulation and
485 handling rather than advancement of the braincase over bulky, less mobile prey, consequently
486 creating different patterns of integration involving areas of attachment for these or other cephalic
487 muscles. The degree to which prey properties, particularly shape or bulkiness, affects patterns of
488 integration in the feeding system of snakes by reorganizing the relative importance of different,
489 overlapping, functional modules should be investigated in further detail. Additionally, the
490 alternative modes of prey ingestion adapted to a broad range of prey types (e.g., mandibular raking,
491 Deufel & Cundall 2003, or sawing, Kojima et al. 2020, or tearing prey, Jayne et al. 2018) illustrates
492 the interspecific variation in myological and functional relationships between the feeding bones.
493 Future studies should examine intraspecific modularity in a select number of taxa at
494 phylogenetically and ecologically informative positions to control for this variation in functional
495 modularity, and to further incorporate within-bone modularity into hypotheses of modularity of
496 the whole feeding system. Accompanying these morphometric analyses with empirical
497 measurements of functional performance (e.g., manipulation and swallowing durations) will
498 provide a better understanding of the factors shaping patterns of integration and modularity in the
499 feeding bones of snakes, specifically how shifting functional relationships between anatomical
500 regions translate into phenotypic covariance.

501 *Morphological integration in the maxilla and upper jaw*

502 The placement of the maxilla in either the palatopterygoid arch module, the suspensorium
503 module, or as an independent module is not apparently clear. Cundall (1983) argued for a medial
504 swallowing functional module, composed of the palatopterygoid arch, and a lateral prey capture
505 functional module, composed of the maxilla and ectopterygoid, in the upper jaw. This functional
506 modularity hypothesis is supported in the local superimposition but not common superimposition
507 results, as the two functional modules are integrated together in the two most supported hypotheses
508 of the common superimposition. The functional dissociation between the lateral and medial upper
509 jaw was noted by Cundall (1983) because the maxilla plays a minimal direct role in ingestion. Yet,

510 the morphological integration between the two suggested modules does not prevent the bones to
511 be involved in different functions. Moreover, the maxilla articulates with the palatine and the
512 ectopterygoid, which articulates with the pterygoid, and the presence of maxillary fangs
513 dramatically restructures the morphology of the maxilla such that some ‘advanced’
514 (alethinophidian) snakes ingest prey using different mechanisms such as mandibular adduction
515 because of the biomechanical limitations from modified cranial morphology due to the presence
516 of maxillary fangs (Deufel and Cundall 2003). A modification in the morphology of the maxilla
517 may then necessarily correspond with modifications in the other elements of the upper jaw because
518 of these articulations, promoting integration within the upper jaw. This is especially true when
519 considering positional information as in the common superimposition but is also captured in PLS1
520 of the maxilla-palatine integration, which shows that shape covariation between the two bones is
521 dominated by their common joint surfaces (Fig. 4). So, while the upper jaw may behave as an
522 evolutionary module, the maxilla and ectopterygoid’s incorporation into this module may be
523 because of structural and physical associations with the palatopterygoid arch, rather than purely
524 functional relationships. This is an important point because morphological integration caused by
525 structural associations between bones is certainly present in the feeding system of snakes, however
526 particularly structurally integrated, fused structures such as the avian cranium show highly
527 complex patterns of modularity (seven modules, Felice & Goswami 2018) despite morphological
528 evolution in one bone necessarily involving the evolution of neighboring bones because they must
529 fit together. Yet, in the hyperkinetic snake feeding apparatus, the most supported hypotheses of
530 modularity describe two to four modules out of eight completely unfused bones.

531 *Modularity and superimposition procedures*

532 Comparing shape (co)variation of a common superimposition and local superimpositions
533 enabled us to analyze separate mobile elements simultaneously and compare the strengths and
534 weaknesses of each method for analyzing modularity. The presence of the maxilla in different
535 modules depending on which superimposition method is used demonstrates the influence that
536 incorporating positional information (GPA_{all}) or isolating pure shape variation (local
537 superimpositions) has when examining patterns of morphological modularity. The maxilla’s
538 integration with the suspensorium when only considering pure shape variation (local
539 superimpositions) is corroborated in PLS1 shape variation of the dentary, quadrate, maxilla, and
540 ectopterygoid, which all showed consistent patterns of shape covariation with one another such

541 that a robust dentary and maxilla, a quadrate with a wider proximal end, and a slender
542 ectopterygoid lied at similar ends of PLS1, as did the combination of a slender dentary and maxilla,
543 a slender and longer quadrate, and a wider anterior ectopterygoid (Fig. 4). This collection of bones
544 that covary along consistent axes of shape covariation with each other may reflect a functional
545 tradeoff between snakes adapted for elusive versus hard-bodied prey; a robust dentary and maxilla
546 is better suited for prey capture than manipulation or ingestion, and a wider proximal quadrate
547 provides additional area for attachment of the mandibular adductor muscle which may increase
548 bite force (Fig. 1A). Comparing superimposition methods revealed competing factors contributing
549 to the maxilla's integration within the feeding system: local superimpositions revealed shared
550 functional selective pressures integrating the maxilla with the suspensorium, and common
551 superimposition revealed structural associations integrating the maxilla with the palatopterygoid
552 arch. The fact that the common superimposition dataset showed a higher magnitude of overall
553 morphological integration than the local superimposition dataset suggests that incorporating
554 positional information contributed to the magnitude of integration (Supplementary Table 1).
555 Allometry also had a greater effect on the common superimposition dataset, possibly due to
556 backwards rotation of the quadrate dominating variation in landmark coordinates.

557 Although the different superimposition methods do not support the same first hypothesis of
558 modularity, both methods strongly support Hypothesis 15 (Fig. 5, 6), describing four modules with
559 relatively distinct functional roles. In this hypothesis of modularity, the palatopterygoid arch
560 including the ectopterygoid form a module, driven by the highly conserved translational movement
561 of the palatopterygoid arch during the pterygoid walk. The maxilla evolves as an individual
562 module, possibly due to the competing structural versus functional influences explained above.
563 The mandible is another module, highly integrated via selection for mechanical advantage. The
564 quadrate and supratemporal, which articulate the feeding apparatus with the braincase, form the
565 last module in this hypothesis, most likely coupled by a shared selective pressure for gape size.
566 While the mandible also contributes to gape size, it is highly constrained by mechanical advantage
567 as discussed above, and the backwards rotation of the quadrate dominates PC1 of the common
568 superimposition (describing nearly half of the total shape variation, Fig. 1B), which is plausibly
569 how, more specifically, a larger gape size is accomplished, thus making the quadrate and
570 supratemporal its own evolutionary module. Further, the largest degree of evolutionary allometry
571 was found in the quadrate; Palci and colleagues (2020) did not find significant evolutionary

572 allometry in the quadrates when considering all Squamata, so the allometry found here likely relates
573 to gape size and is adaptive.

574 Since different integration-inducing functional, developmental, and genetic processes may
575 affect shape, positional, and size variation unevenly, our use of common and local
576 superimpositions attempts to bracket the ‘true’ pattern of modularity. Moreover, eigenvalue
577 dispersion and 2BPLS results, which are independent of rotational and positional variation, were
578 largely consistent with CR results. H15 is possibly the pattern in which component parts of the
579 feeding system evolve semi-independently, as both superimposition methods strongly support it,
580 however there may exist an even less complex pattern of modularity considering that two-module
581 hypotheses were most supported in both methods.

582 *Does the magnitude of morphological integration constrain morphological diversity?*

583 Previous work has shown that the strength of integration can facilitate (Navalon et al. 2020;
584 Fabre et al. 2020; Randau & Goswami 2017a), constrain (Goswami & Polly 2010b; Felice et al.
585 2018), or have no recoverable effect on morphological diversity (paedomorphic salamanders in
586 Fabre et al. 2020; Bardua et al. 2019b; Watanabe et al. 2019; Bon et al. 2020). Here, we find that
587 neither the strength of within-bone integration nor the average strength of each bone’s association
588 with another has a significant effect on morphological diversity (Fig. 3B). As such, the
589 considerably high degree of integration within the feeding system of aquatic-foraging snakes does
590 not seem to affect morphological diversity over macroevolutionary timescales. This finding is
591 interesting when considering the ecological and functional diversity of aquatic-foraging snakes, as
592 it indicates that sufficient mechanical solutions to a broad range of feeding behaviors and diets are
593 readily accessible within the highly integrated hyperkinetic feeding system of aquatic-foraging
594 snakes.

595 *The hyperkinetic feeding system is highly integrated*

596 Despite the kinesis in the feeding system of snakes, the individual bones are highly integrated
597 with one another and organize into two to four evolutionary modules (Fig. 5, 6). In fact, the
598 extreme kinesis is the reason why the feeding systems of snakes is so functionally optimized and
599 thus so highly integrated (Cundall and Greene 2000; Moon et al. 2019). The developmental
600 disintegration necessary to anatomically liberate fused structures implies that snake feeding bones
601 oppose an expectation in morphological integration and modularity literature which suggests that

602 functional systems may adaptively evolve in congruence with developmental systems or vice versa
603 (Cheverud 1984, 1996; Wagner & Altenberg 1996; Klingenberg 2014). Of course, this does not
604 consider alternative modes of developmental integration between separate bones, such as shared
605 gene expressions, pleiotropic effects, or shared embryonic origin. Developmental systems can
606 integrate spatially separated features as well, such as serially homologous limb bones
607 (Hallgrímsson et al. 2002; Bell et al. 2011) or vertebrae (Randau & Goswami 2017a, b, 2018;
608 Jones et al. 2018, 2020; Arlegi et al. 2020). Accordingly, it is possible that the evolutionary and
609 functional modules of H15 (Fig. 5, 6) also match some pattern of developmental or genetic
610 modularity. In any case, our developmental modularity hypotheses, which considered the
611 embryonic origins of the articular and quadrate (splanchnocranium) and the rest of the feeding
612 bones (dermatocranium), were not well supported (Supplementary Table 5). While additional
613 patterns of developmental integration potentially contributing to morphological integration in the
614 snake skull are less understood but surely exist, the high amount morphological integration in the
615 kinetic feeding system of snakes is striking when considering the complex patterns of modularity
616 recovered from the synostotic bones that make up akinetic morphological structures in mammals
617 (Goswami 2006; Martín-Serra et al. 2018; Adams & Collyer 2019), archosaurs (Felice and
618 Goswami 2018; Felice et al. 2019), and amphibians (Marshall et al. 2019; Bardua et al. 2019; Bon
619 et al. 2020; Fabre et al. 2020). In the feeding system of aquatic-foraging snakes, we recognize
620 strong functional and evolutionary integration generated because of its kinesis and developmental
621 disintegration.

622 **Conclusion**

623 In this paper, we quantify shape variation in the hyperkinetic feeding system of a
624 phylogenetically broad sample of aquatic-foraging snakes and review patterns of morphological
625 integration and modularity within this system. We find that the feeding system is highly integrated,
626 with the most supported hypotheses of modularity involving only two modules despite there being
627 eight separate bones unfused with one another. The most supported patterns of modularity describe
628 an integrated palatopterygoid arch and mandible as separate modules, with the maxilla and
629 quadrate either part of the palatopterygoid arch or mandible module depending on whether
630 positional information was preserved in the superimposition method. Regardless, both
631 superimposition methods show strong support for a four-module hypothesis with each separate
632 module responsible for a specific functional role. This four-module hypothesis may be the best

633 representation of how different regions of the feeding system independently evolve. Indeed, the
634 major axes of phylogenetic-corrected shape variation of each of these modules have considerable
635 functional consequences (Fig. 6), suggesting that modularity and integration is primarily
636 influenced by performance-based selective pressures associated with feeding ecology. The utility
637 of comparing common and local superimpositions of a mobile system to ‘bracket’ the most
638 biologically accurate pattern of modularity proved fruitful and may be considered in future studies
639 when taking appropriate precautions. Further, the relatively high degree of integration in this
640 hyperkinetic system is fascinating when considering the developmental disintegration necessary
641 to spatially disintegrate each component part, and the complex patterns of modularity found in
642 fused structures such as rodent mandibles (Adams & Collyer 2019). Despite this exceptionally
643 strong integration within the feeding system, morphological diversity is not apparently
644 constrained, indicating that adequate mechanical and functional solutions to a wide variety of
645 dietary and ecological niches are readily available within constraint due to integration in the
646 feeding system. Further research addressing morphological integration in the skull of snakes with
647 different dietary challenges (e.g. arboreal species, snail-eaters, egg-eaters) should be conducted to
648 reveal the relative importance of competing functional, developmental, and genetic factors
649 influencing morphological integration and their micro- and macroevolutionary consequences.

650 **Acknowledgments**

651 We thank the herpetological collections staff of the American Museum of Natural History: David Kizirian,
652 David Dickey, Margaret Arnold and especially Lauren Vonnahme, but also Alan Resetar (Field Museum
653 of Natural History), Erica Ely and Lauren Scheinberg (California Academy of Sciences) for their help and
654 patience in carefully choosing specimens that fit our study and quickly processing specimen loans. Another
655 special thanks to Morgan Hill Chase and Andrew Smith, from the Microscopy and Imaging and Facility
656 who did all the CT scanning involved in this study. The authors greatly appreciate insightful comments by
657 Spencer Hellert that improved earlier versions of this manuscript. We thank the National Science
658 Foundation REU program and the Fyssen Foundation for partly funding this research.

659 **Author contributions**

660 DR contributed to the data acquisition, analysis, interpretation of the results, writing and editing. DP and
661 CR contributed to the interpretation and discussion of the results, as well as the review and edits of the
662 manuscript. MS conceived the study, generated the scans, helped in the analyses, the interpretation of results
663 and reviewed the manuscript.

664 References

- 665 Adams, D. C. (1999). Methods for shape analysis of landmark data from articulated structures. *Evolutionary*
666 *Ecology Research*, 1(8), 959-970.
- 667 Adams, D. C., & Rohlf, F. J. (2000). Ecological character displacement in Plethodon: biomechanical
668 differences found from a geometric morphometric study. *Proceedings of the National Academy of*
669 *Sciences*, 97(8), 4106-4111.
- 670 Adams, D. C. (2004). Character displacement via aggressive interference in Appalachian salamanders.
671 *Ecology*, 85(10), 2664-2670.
- 672 Adams, D. C., Rohlf, F. J., & Slice, D. E. (2004). Geometric morphometrics: ten years of progress following
673 the 'revolution'. *Italian Journal of Zoology*, 71(1), 5-16.
- 674 Adams, D. C., Rohlf, F. J., & Slice, D. E. (2013). A field comes of age: geometric morphometrics in the
675 21st century. *Hystrix*, 24(1), 7.
- 676 Adams, D. C. (2014). A generalized K statistic for estimating phylogenetic signal from shape and other
677 high-dimensional multivariate data. *Systematic Biology*, 63(5), 685-697.
- 678 Adams, D. C., & Felice, R. N. (2014). Assessing trait covariation and morphological integration on
679 phylogenies using evolutionary covariance matrices. *PloS one*, 9(4), e94335.
- 680 Adams, D. C. (2016). Evaluating modularity in morphometric data: challenges with the RV coefficient and
681 a new test measure. *Methods in Ecology and Evolution*, 7(5), 565-572.
- 682 Adams, D. C., & Collyer, M. L. (2016). On the comparison of the strength of morphological integration
683 across morphometric datasets. *Evolution*, 70(11), 2623-2631.
- 684 Adams, D. C., & Otárola-Castillo, E. (2013). geomorph: an R package for the collection and analysis of
685 geometric morphometric shape data. *Methods in Ecology and Evolution*, 4(4), 393-399.
- 686 Adams, D. C., & Collyer, M. L. (2018). Multivariate phylogenetic comparative methods: evaluations,
687 comparisons, and recommendations. *Systematic biology*, 67(1), 14-31.
- 688 Adams, D. C., & Collyer, M. L. (2019). Comparing the strength of modular signal, and evaluating
689 alternative modular hypotheses, using covariance ratio effect sizes with morphometric
690 data. *Evolution*, 73(12), 2352-2367.
- 691 Andjelković, M., Tomović, L., & Ivanović, A. (2016). Variation in skull size and shape of two snake species
692 (*Natrix natrix* and *Natrix tessellata*). *Zoomorphology*, 135(2), 243-253.
- 693 Andjelković, M., Tomović, L., & Ivanović, A. (2017). Morphological integration of the kinetic skull in
694 Natrix snakes. *Journal of Zoology*, 303(3), 188-198.
- 695 Atchley, W. R., & Hall, B. K. (1991). A model for development and evolution of complex morphological
696 structures. *Biological Reviews*, 66(2), 101-157.
- 697 Arlegi, M., Veschambre-Couture, C., & Gómez-Olivencia, A. (2020). Evolutionary selection and
698 morphological integration in the vertebral column of modern humans. *American journal of physical*
699 *anthropology*, 171(1), 17-36.
- 700 Bardua, C., Felice, R. N., Watanabe, A., Fabre, A. C., & Goswami, A. (2019a). A practical guide to sliding
701 and surface semilandmarks in morphometric analyses. *Integrative Organismal Biology*, 1(1),
702 obz016.
- 703 Bardua, C., Wilkinson, M., Gower, D. J., Sherratt, E., & Goswami, A. (2019b). Morphological evolution
704 and modularity of the caecilian skull. *BMC evolutionary biology*, 19(1), 30.
- 705 Bell, E., Andres, B., & Goswami, A. (2011). Integration and dissociation of limb elements in flying
706 vertebrates: a comparison of pterosaurs, birds and bats. *Journal of evolutionary biology*, 24(12),
707 2586-2599.
- 708 Boltz, R. E., & Ewer, R. F. (1964). The functional anatomy of the head of the puff adder, *Bitis arietans*
709 (Merr.). *Journal of Morphology*, 114(1), 83-105.
- 710 Bon, M., Bardua, C., Goswami, A., & Fabre, A. C. (2020). Cranial integration in the fire salamander,
711 *Salamandra salamandra* (Caudata: Salamandridae). *Biological Journal of the Linnean*
712 *Society*, 130(1), 178-194.

- 713 Boughner, J. C., Buchtová, M., Fu, K., Diewert, V., Hallgrímsson, B., & Richman, J. M. (2007). Embryonic
714 development of *Python sebae*—I: Staging criteria and macroscopic skeletal morphogenesis of the
715 head and limbs. *Zoology*, *110*(3), 212-230.
- 716 Caldwell, M. W. (2019). *The Origin of Snakes: Morphology and the Fossil Record*. Boca Raton: CRC
717 Press, 2019. doi:10.1201/9781315118819.
- 718 Cheverud, J. M. (1984). Quantitative genetics and developmental constraints on evolution by
719 selection. *Journal of theoretical biology*, *110*(2), 155-171.
- 720 Cheverud, J. M. (1996). Developmental integration and the evolution of pleiotropy. *American*
721 *Zoologist*, *36*(1), 44-50.
- 722 Collyer, M. L., Davis, M. A., & Adams, D. C. (2020). Making Heads or Tails of Combined Landmark
723 Configurations in Geometric Morphometric Data. *Evolutionary Biology*, *47*(1), 193-204
- 724 Cundall, D. (1983). Activity of head muscles during feeding by snakes: a comparative study. *American*
725 *Zoologist*, *23*(2), 383-396.
- 726 Cundall, D., & Greene, H. W. (2000). Feeding in snakes. *Feeding: form, function, and evolution in tetrapod*
727 *vertebrates*, Elsevier. 293-333.
- 728 Deufel, A., & Cundall, D. (2003). Feeding in Atractaspis (Serpentes: Atractaspididae): a study in conflicting
729 functional constraints. *Zoology*, *106*(1), 43-61.
- 730 dos Santos, M. M., da Silva, F. M., Hingst-Zaher, E., Machado, F. A., Zaher, H. E. D., & da Costa Prudente,
731 A. L. (2017). Cranial adaptations for feeding on snails in species of *Sibynomorphus* (Dipsadidae:
732 Dipsadinae). *Zoology*, *120*, 24-30.
- 733 Dumont, M., Wall, C. E., Botton-Divet, L., Goswami, A., Peigné, S., & Fabre, A. C. (2016). Do functional
734 demands associated with locomotor habitat, diet, and activity pattern drive skull shape evolution in
735 musteloid carnivorans? *Biological Journal of the Linnean Society*, *117*(4), 858-878.
- 736 Esquerré, D., Sherratt, E., & Keogh, J. S. (2017). Evolution of extreme ontogenetic allometric diversity and
737 heterochrony in pythons, a clade of giant and dwarf snakes. *Evolution*, *71*(12), 2829-2844.
- 738 Fabre, A. C., Bickford, D., Segall, M., & Herrel, A. (2016). The impact of diet, habitat use, and behaviour
739 on head shape evolution in homalopsid snakes. *Biological Journal of the Linnean Society*, *118*(3),
740 634-647.
- 741 Fabre, A. C., Bardua, C., Bon, M., Clavel, J., Felice, R. N., Streicher, J. W., ... & Goswami, A. (2020).
742 Metamorphosis shapes cranial diversity and rate of evolution in salamanders. *Nature Ecology &*
743 *Evolution*, *4*(8), 1129-1140.
- 744 Felice, R. N., Randau, M., & Goswami, A. (2018). A fly in a tube: Macroevolutionary expectations for
745 integrated phenotypes. *Evolution*, *72*(12), 2580-2594.
- 746 Felice, R. N., & Goswami, A. (2018). Developmental origins of mosaic evolution in the avian
747 cranium. *Proceedings of the National Academy of Sciences*, *115*(3), 555-560.
- 748 Felice, R. N., Watanabe, A., Cuff, A. R., Noirault, E., Pol, D., Witmer, L. M., ... & Goswami, A. (2019).
749 Evolutionary integration and modularity in the archosaur cranium. *Integrative and comparative*
750 *biology*, *59*(2), 371-382.
- 751 Goswami, A. (2006). Cranial modularity shifts during mammalian evolution. *The American*
752 *Naturalist*, *168*(2), 270-280.
- 753 Goswami, A., & Polly, P. D. (2010a). Methods for studying morphological integration and modularity. *The*
754 *Paleontological Society Papers*, *16*, 213-243.
- 755 Goswami, A., & Polly, P. D. (2010b). The influence of modularity on cranial morphological disparity in
756 Carnivora and Primates (Mammalia). *PloS one*, *5*(3), e9517.
- 757 Goswami, A., Smaers, J. B., Soligo, C., & Polly, P. D. (2014). The macroevolutionary consequences of
758 phenotypic integration: from development to deep time. *Philosophical Transactions of the Royal*
759 *Society B: Biological Sciences*, *369*(1649), 20130254.
- 760 Goswami, A., Watanabe, A., Felice, R. N., Bardua, C., Fabre, A. C., & Polly, P. D. (2019). High-density
761 morphometric analysis of shape and integration: the good, the bad, and the not-really-a-
762 problem. *Integrative and Comparative Biology*, *59*(3), 669-683.

- 763 Gunz, P., Mitteroecker, P., & Bookstein, F. L. (2005). Semilandmarks in three dimensions. *Modern*
764 *morphometrics in physical anthropology*, Springer. 73-98.
- 765 Gunz, P., & Mitteroecker, P. (2013). Semilandmarks: a method for quantifying curves and
766 surfaces. *Hystrix, the Italian Journal of Mammalogy*, 24(1), 103-109.
- 767 Hallgrímsson, B., Jamniczky, H., Young, N. M., Rolian, C., Parsons, T. E., Boughner, J. C., & Marcucio,
768 R. S. (2009). Deciphering the palimpsest: studying the relationship between morphological
769 integration and phenotypic covariation. *Evolutionary biology*, 36(4), 355-376.
- 770 Hallgrímsson, B., Willmore, K., & Hall, B. K. (2002). Canalization, developmental stability, and
771 morphological integration in primate limbs. *American Journal of Physical*
772 *Anthropology*, 119(S35), 131-158.
- 773 Hampton, P. M. (2011). Comparison of cranial form and function in association with diet in natricine
774 snakes. *Journal of Morphology*, 272(12), 1435-1443.
- 775 Jackson, K. (2003). The evolution of venom-delivery systems in snakes. *Zoological Journal of the Linnean*
776 *Society*, 137(3), 337-354.
- 777 Jayne BC, Voris HK, Ng PKL. 2018 How big is too big? Using crustacean-eating snakes (Homalopsidae)
778 to test how anatomy and behaviour affect prey size and feeding performance. *Biol. J. Linn. Soc.*
779 *123*(3), 636–650.
- 780 Jayne, B. C., Voris, H. K., & Ng, P. K. L. (2002). Snake circumvents constraints on prey size. *Nature*,
781 *418*(6894), 143–143
- 782 Johnston, P. (2014). Homology of the jaw muscles in lizards and snakes—a solution from a comparative
783 gnathostome approach. *The Anatomical Record*, 297(3), 574-585.
- 784 Jones, K. E., Benitez, L., Angielczyk, K. D., & Pierce, S. E. (2018). Adaptation and constraint in the
785 evolution of the mammalian backbone. *BMC evolutionary biology*, 18(1), 1-13.
- 786 Jones, K. E., Gonzalez, S., Angielczyk, K. D., & Pierce, S. E. (2020). Regionalization of the axial skeleton
787 predates functional adaptation in the forerunners of mammals. *Nature Ecology & Evolution*, 4(3),
788 470-478.
- 789 Kardong, K. V. (1977). Kinesis of the jaw apparatus during swallowing in the cottonmouth snake,
790 *Agkistrodon piscivorus*. *Copeia*, 1977(2), 338-348.
- 791 Kardong, K. V. (1979). 'Protovipers' and the Evolution of Snake Fangs. *Evolution*, 33(1) 433-443.
- 792 Khannoon, E. R., & Evans, S. E. (2015). The development of the skull of the Egyptian cobra *Naja h. haje*
793 (Squamata: Serpentes: Elapidae). *PLoS one*, 10(4), e0122185.
- 794 Klaczko, J., Sherratt, E., & Setz, E. Z. (2016). Are diet preferences associated to skulls shape diversification
795 in xenodontine snakes? *PLoS One*, 11(2), e0148375.
- 796 Klingenberg, C. P. (2008). Morphological integration and developmental modularity. *Annual review of*
797 *ecology, evolution, and systematics*, 39, 115-132.
- 798 Klingenberg, C. P. (2014). Studying morphological integration and modularity at multiple levels: concepts
799 and analysis. *Philosophical Transactions of the Royal Society B: Biological Sciences*, 369(1649),
800 20130249.
- 801 Kojima, Y., Fukuyama, I., Kurita, T., Hossman, M. Y. B., & Nishikawa, K. (2020). Mandibular sawing in
802 a snail-eating snake. *Scientific reports*, 10(1), 1-5.
- 803 Lebrun, R., & Orliac, M. J. (2017). MorphoMuseum: an online platform for publication and storage of
804 virtual specimens. *Paleontology Society Papers*, 22, 183-195.
- 805 Martín-Serra, A., Figueirido, B., & Palmqvist, P. (2020). Changing modular patterns in the carnivoran
806 pelvic girdle. *Journal of Mammalian Evolution*, 27(2), 237-243.
- 807 Marshall, A. F., Bardua, C., Gower, D. J., Wilkinson, M., Sherratt, E., & Goswami, A. (2019). High-density
808 three-dimensional morphometric analyses support conserved static (intraspecific) modularity in
809 caecilian (Amphibia: Gymnophiona) crania. *Biological Journal of the Linnean Society*, 126(4),
810 721-742.
- 811 Melo, D., Porto, A., Cheverud, J. M., & Marroig, G. (2016). Modularity: genes, development, and
812 evolution. *Annual review of ecology, evolution, and systematics*, 47, 463-486.

- 813 Murphy JC. 2012 Marine invasions by non-sea snakes, with thoughts on terrestrial–aquatic– marine
814 transitions. *Integrative and Comparative Biology*, 52, 217–226.
- 815 Mushinsky, H. R., Hebrard, J. J. and Vodopich, D. S. (1982). Ontogeny of water snake foraging ecology.
816 *Ecology* 63(6), 1624-1629.
- 817 Murta-Fonseca, R. A., Machado, A., Lopes, R. T., & Fernandes, D. S. (2019). Sexual dimorphism in
818 *Xenodon neuwiedii* skull revealed by geometric morphometrics (Serpentes;
819 Dipsadidae). *Amphibia-Reptilia*, 40(4), 461-474.
- 820 Moon, B. R., Penning, D. A., Segall, M., & Herrel, A. (2019). Feeding in Snakes: Form, Function, and
821 Evolution of the Feeding System. In *Feeding in Vertebrates* (pp. 527-574). Springer, Cham.
- 822 Mori, A., & Vincent, S. E. (2008). An integrative approach to specialization: relationships among feeding
823 morphology, mechanics, behaviour, performance and diet in two syntopic snakes. *Journal of*
824 *Zoology*, 275(1), 47-56.
- 825 Navalón, G., Marugán-Lobón, J., Bright, J. A., Cooney, C. R., & Rayfield, E. J. (2020). The consequences
826 of craniofacial integration for the adaptive radiations of Darwin’s finches and Hawaiian
827 honeycreepers. *Nature Ecology & Evolution*, 4(2), 270-278.
- 828 Olson, E. C., & Miller, R. L. (1958). *Morphological integration*. University of Chicago Press.
- 829 Palci, A., Lee, M. S., & Hutchinson, M. N. (2016). Patterns of postnatal ontogeny of the skull and lower
830 jaw of snakes as revealed by micro-CT scan data and three-dimensional geometric
831 morphometrics. *Journal of anatomy*, 229(6), 723-754.
- 832 Palci, A., Caldwell, M. W., Hutchinson, M. N., Konishi, T., & Lee, M. S. (2020). The morphological
833 diversity of the quadrate bone in squamate reptiles as revealed by high-resolution computed
834 tomography and geometric morphometrics. *Journal of Anatomy*, 236(2), 210-227.
- 835 Pavlicev, M., Cheverud, J. M., & Wagner, G. P. (2009). Measuring morphological integration using
836 eigenvalue variance. *Evolutionary Biology*, 36(1), 157-170.
- 837 Polachowski, K. M., & Werneburg, I. (2013). Late embryos and bony skull development in *Bothropoides*
838 *jararaca* (Serpentes, Viperidae). *Zoology*, 116(1), 36-63.
- 839 Pyron, R. A. and Burbrink, F. T. (2014). Early origin of viviparity and multiple reversions to oviparity in
840 squamate reptiles. *Ecology Letters* 17(1), 13–21.
- 841 Raff, R. A. (1996). *The shape of life: genes, development, and the evolution of animal form*. University of
842 Chicago Press.
- 843 Randau, M., & Goswami, A. (2017a). Unravelling intravertebral integration, modularity and disparity in
844 Felidae (Mammalia). *Evolution & development*, 19(2), 85-95.
- 845 Randau, M., & Goswami, A. (2017b). Morphological modularity in the vertebral column of Felidae
846 (Mammalia, Carnivora). *BMC evolutionary biology*, 17(1), 133.
- 847 Randau, M., & Goswami, A. (2018). Shape covariation (or the lack thereof) between vertebrae and other
848 skeletal traits in felids: the whole is not always greater than the sum of parts. *Evolutionary*
849 *biology*, 45(2), 196-210.
- 850 Revell, L. J. (2009). Size-correction and principal components for interspecific comparative
851 studies. *Evolution*, 63(12), 3258-3268.
- 852 Rohlf, F. J., & Slice, D. (1990). Extensions of the Procrustes method for the optimal superimposition of
853 landmarks. *Systematic Biology*, 39(1), 40-59.
- 854 Rohlf, F. J., & Corti, M. (2000). Use of two-block partial least-squares to study covariation in
855 shape. *Systematic Biology*, 49(4), 740-753.
- 856 Savitzky, A. H. (1983). Coadapted character complexes among snakes: fossoriality, piscivory, and
857 durophagy. *American Zoologist* 23(2), 397–409.
- 858 Scanferla, A. (2016). Postnatal ontogeny and the evolution of macrostomy in snakes. *Royal Society open*
859 *science*, 3(11), 160612.
- 860 Schlager, S. (2017). Morpho and Rvcg–Shape Analysis in R: R-Packages for geometric morphometrics,
861 shape analysis and surface manipulations. In *Statistical shape and deformation analysis* (pp. 217-
862 256). Academic Press.

- 863 Sherratt, E., Sanders, K. L., Watson, A., Hutchinson, M. N., Lee, M. S., & Palci, A. (2019). Heterochronic
864 shifts mediate ecomorphological convergence in skull shape of microcephalic sea
865 snakes. *Integrative and comparative biology*, 59(3), 616-624.
- 866 Segall, M., Cornette, R., Fabre, A. C., Godoy-Diana, R., & Herrel, A. (2016). Does aquatic foraging impact
867 head shape evolution in snakes? *Proceedings of the Royal Society B: Biological
868 Sciences*, 283(1837), 20161645.
- 869 Segall, M., Herrel, A., & Godoy-Diana, R. (2019). Hydrodynamics of frontal striking in aquatic snakes:
870 drag, added mass, and the possible consequences for prey capture success. *Bioinspiration &
871 biomimetics*, 14(3), 036005.
- 872 Segall, M., Cornette, R., Godoy-Diana, R., & Herrel, A. (2020). Exploring the functional meaning of head
873 shape disparity in aquatic snakes. *Ecology and Evolution*, 10(14), 6993–7005.
- 874 Sheverdyukova, H. V. (2019). Development of the Osteocranium in *Natrix natrix* (Serpentes, Colubridae)
875 Embryogenesis II: Development of the jaws, palatal complex and associated bones. *Acta
876 Zoologica*, 100(3), 282-291.
- 877 Silva, F. M., Prudente, A. L. D. C., Machado, F. A., Santos, M. M., Zaher, H., & Hingst-Zaher, E. (2018).
878 Aquatic adaptations in a Neotropical coral snake: A study of morphological convergence. *Journal
879 of Zoological Systematics and Evolutionary Research*, 56(3), 382-394.
- 880 Souto, N. M., Murta-Fonseca, R. A., Machado, A. S., Lopes, R. T., & Fernandes, D. S. (2019). Snakes as
881 a model for measuring skull preparation errors in geometric morphometrics. *Journal of
882 Zoology*, 309(1), 12-21.
- 883 Uetz, P., Cherikh, S., Shea, G., Ineich, I., Campbell, P. D., Doronin, I. V., ... & Lee, J. L. (2019). A global
884 catalog of primary reptile type specimens. *Zootaxa*, 4695(5), 438-450.
- 885 Vincent, S. E., Moon, B. R., Herrel, A., & Kley, N. J. (2007). Are ontogenetic shifts in diet linked to shifts
886 in feeding mechanics? Scaling of the feeding apparatus in the banded watersnake *Nerodia
887 fasciata*. *Journal of Experimental Biology*, 210(12), 2057-2069.
- 888 Wagner, G. P., & Altenberg, L. (1996). Perspective: complex adaptations and the evolution of
889 evolvability. *Evolution*, 50(3), 967-976.
- 890 Wagner, G. P., Pavlicev, M., & Cheverud, J. M. (2007). The road to modularity. *Nature Reviews
891 Genetics*, 8(12), 921-931.
- 892 Wainwright, P. C., & Richard, B. A. (1995). Predicting patterns of prey use from morphology of
893 fishes. *Environmental Biology of Fishes*, 44(1-3), 97-113.
- 894 Watanabe, A., Fabre, A. C., Felice, R. N., Maisano, J. A., Müller, J., Herrel, A., & Goswami, A. (2019).
895 Ecomorphological diversification in squamates from conserved pattern of cranial
896 integration. *Proceedings of the National Academy of Sciences*, 116(29), 14688-14697.
- 897 Werneburg, I., Polachowski, K. M., & Hutchinson, M. N. (2015). Bony skull development in the Argus
898 monitor (Squamata, Varanidae, *Varanus panoptes*) with comments on developmental timing and
899 adult anatomy. *Zoology*, 118(4), 255-280.
- 900 Wiley, D. F., Amenta, N., Alcantara, D. A., Ghosh, D., Kil, Y. J., Delson, E., ... & Hamann, B. (2005,
901 October). Evolutionary morphing. In *VIS 05. IEEE Visualization, 2005*. (pp. 431-438). IEEE.

902 **Supplementary Tables & Figures**

903 Supplementary Table 1. Species and specimens used in this study. Museum codes: AMNH – American Museum of
 904 Natural History, FMNH – Field Museum of Natural History, CAS – California Academy of Sciences. Topology of
 905 the phylogeny used in this paper, from Pyron & Burbrink (2014).

Phylogeny	Scientific Name	Specimen Numbers	
Colubridae	<i>Hydrodynastes gigas</i>	AMNH R60031, AMNH R93649	
	<i>Helicops carinicaudus</i>	CAS87097	
	<i>Helicops angulatus</i>	AMNH R130927, AMNH R18150	
	<i>Hydrops triangularis</i>	AMNH R22449	
	<i>Pseudoeryx plicatilis</i>	AMNH R55335	
	<i>Thamnophis atratus</i>	AMNH R162404, AMNH R162405	
	<i>Thamnophis couchii</i>	AMNH R09839, AMNH R09840	
	<i>Nerodia sipedon</i>	AMNH R17086, AMNH R175012	
	<i>Nerodia rhombifer</i>	AMNH R162256, AMNH R46754, AMNH R153729, AMNH R153727	
	<i>Liodytes rigida</i>	AMNH R160212	
	<i>Liodytes alleni</i>	AMNH R159304	
	<i>Xenochrophis piscator</i>	AMNH R34085, AMNH R34086	
	<i>Hydrophis ornatus</i>	AMNH R116013, AMNH R66588	
	<i>Hydrophis schistosus</i>	AMNH R81854, CAS12296	
Elapidae	<i>Hydrophis platurus</i>	AMNH R19316, AMNH R19329	
	<i>Hydrophis melanocephalus</i>	AMNH R03901, CAS22122	
	<i>Hydrelaps darwiniensis</i>	AMNH R86169	
	<i>Aipysurus laevis</i>	AMNH R161752, AMNH R5087	
	<i>Laticauda colubrina</i>	AMNH R28997, AMNH R29000	
	<i>Micrurus lemniscatus</i>	AMNH R119215	
	<i>Micrurus surinamensis</i>	AMNH R152339	
	Homalopsidae	<i>Cerberus rynchops</i>	AMNH R161961, FMNH199678, FMNH203432
		<i>Homalopsis buccata</i>	AMNH R92297, FMNH183771, FMNH229816
		<i>Gerarda prevostiana</i>	FMNH179104
<i>Fordonia leucobalia</i>		FMNH229751, FMNH229758, FMNH229748	
<i>Cantoria violacea</i>		FMNH250116, CAS211909, CAS211910	
<i>Myron richardsonii</i>		AMNH R111792, AMNH R111793	
<i>Erpeton tentaculatum</i>		FMNH252609, FMNH252504	
<i>Subessor bocourti</i>		FMNH191113, FMNH263528	
Acrochordidae	<i>Acrochordus arafurae</i>	CAS122071, CAS135488	
Cylindrophiiidae	<i>Cylindrophis ruffus</i>	CAS16847	
Boidae	<i>Eunectes murinus</i>	AMNH R56132, AMNH R46336	

906

907 Supplementary Table 2. Explanations for each alternative hypothesis of modularity.

#	Hypothesis	Explanation
1	[dentary, compound] + [else]	Cranial elements and mandibular elements as separate evolutionary modules. Dorsal-ventral modularity.
2	[dentary, compound, quadrate, supratemporal] + [pterygoid, palatine, ectopterygoid, maxilla]	Suspensorium module consisting of the mandible, quadrate, and supratemporal and an upper jaw module. The mandible, quadrate, and supratemporal cumulatively contribute to gape size, which dictates the maximum size of prey (Cundall & Greene 2000). The elements of the suspensorium must act in concert to successfully strike at prey (Cundall & Greene 2000; Moon et al. 2019).
3	[maxilla, ectopterygoid] + [else]	The maxilla is not functionally integrated as strongly as the other bones (Cundall 1983), however the presence of fangs restructures its morphology and function (Kardong 1979; Vonk et al. 2008), and it may be integrated with the ectopterygoid because they articulate.
4	[dentary, compound, quadrate, maxilla] + [supratemporal, pterygoid, palatine, ectopterygoid]	Lateral vs. medial modules
5	[dentary, anterior compound] + [else]	Same as hypothesis #1 but with developmental modularity in compound. The posterior compound and quadrate are splanchnocranial.
6	[pterygoid, palatine] + [else]	Two-module hypothesis with the palatopterygoid arch as an individual module. The pterygoid and palatine articulate to make the palatopterygoid arch, which is necessary for the successfully functioning of the 'pterygoid walk' (Boltz and Ewer 1964).
7	[quadrate, supratemporal] + [else]	The quadrate's size and relative orientation varies greatly among species, and it is the only bone involved in prey detection as it connects to the stapes. The supratemporal is articulated with the quadrate and its relative position also varies greatly across the dataset.
8	[posterior compound, quadrate, supratemporal] + [else]	Developmental modularity; the quadrate and articular of the compound (posterior compound) are splanchnocranial, the other bones are dermatocranial.
9	[dentary, compound] + [quadrate, supratemporal] + [pterygoid, palatine, ectopterygoid, maxilla]	Same as hypothesis #1 and #2, but with the quadrate and supratemporal as an individual module. The relative orientation of the quadrate varies greatly among species, which has biomechanical implications (Scanferla 2016).
10	[dentary, compound, quadrate, supratemporal] + [maxilla] + [pterygoid, palatine, ectopterygoid]	Same as hypothesis #2, but with the mandible (suspensorium) as an individual module.
11	[dentary, compound, quadrate, supratemporal] + [maxilla, ectopterygoid] + [pterygoid, palatine]	Same as hypothesis #11, but with the ectopterygoid integrated with the maxilla, because they articulate.
12	[dentary, maxilla] + [compound, quadrate, supratemporal] + [pterygoid, palatine, ectopterygoid]	The dentary and maxilla are tooth bearing bones which are in direct physical contact with prey during prey capture (Cundall 1983; Cundall & Greene 2000; Moon et al. 2019). The compound and quadrate are connected via the mandibular adductor, which originates on the anterior quadrate and inserts on the posterolateral compound (Johnston 2014). The palatopterygoid arch articulates with the ectopterygoid.
13	[dentary, compound, maxilla, ectopterygoid] + [quadrate, supratemporal] + [pterygoid, palatine]	Same as hypothesis #11, but with the compound and ectopterygoid in the same module as the dentary and maxilla because they articulate with the dentary and maxilla, respectively.
14	[dentary, anterior compound] + [posterior compound, quadrate, supratemporal] + [pterygoid, palatine, ectopterygoid, maxilla]	Same as hypothesis #9 but incorporating developmental modularity in the compound.
15	[dentary, compound] + [quadrate, supratemporal] + [pterygoid, palatine, ectopterygoid] + [maxilla]	Same as hypothesis #9, but with the maxilla as an individual module. The maxilla has little direct role in any functional module other than prey capture in many species (Cundall 1983).
16	[dentary, compound] + [quadrate, supratemporal] + [pterygoid, palatine] + [maxilla, ectopterygoid]	Same as hypothesis #15, but with the ectopterygoid in the maxilla module.
17	[dentary, anterior compound] + [posterior compound, quadrate, supratemporal] + [pterygoid, palatine] + [ectopterygoid, maxilla]	Same as hypothesis #16, but modularity within compound.
18	Complete modularity except [pterygoid, palatine] + [dentary, compound]	The mandible and palatopterygoid arch are hypothesized to be two of the most integrated pairs of bones. This hypothesis considers modularity except for these two structures.
19	Complete modularity except [pterygoid, palatine]	Same as hypothesis #5, but with complete modularity outside of the palatopterygoid arch.
20	Complete modularity except [dentary, compound]	The mandibular elements are expected to be integrated because of their articulation and functional relationships; are mandibular, but not cranial elements integrated?
21	Complete modularity	The separate bones are unfused with one another, potentially allowing one bone to evolve without the necessary evolution of another. Does cranial kinesis promote modularity?

908 Supplementary Table 3. The influence of allometry, phylogeny, and integration on snake skull bones associated with
 909 feeding. Results of allometry (PGLS), phylogenetic signal (all significant; $0.001 < p < 0.004$), and eigenvalue
 910 dispersion analyses. Significant p-values of allometry analyses are in bold. Higher eigenvalue dispersion value
 911 corresponds to higher degrees of overall integration within each structure. That is, more integrated structures will have
 912 more correlated shape variation consolidated in the first few principal components (eigenvalues).

Structure	Allometry		Phylogenetic Signal		Integration
	R ²	P	K	Effect Size	Eigenvalue dispersion
Dentary	0.06	0.15	0.45	2.99	0.61
Compound	0.08	0.051	0.58	3.91	0.65
Quadrate	0.26	0.001	0.51	3.05	0.55
Supratemporal	0.08	0.02	0.47	3.76	0.45
Pterygoid	0.07	0.09	0.51	3.04	0.47
Ectopterygoid	0.03	0.39	0.38	3.13	0.65
Palatine	0.08	0.02	0.59	5.97	0.48
Maxilla	0.07	0.03	0.57	4.63	0.47
Common Superimposition	0.13	0.001	0.48	4.20	0.45
Local Superimpositions	0.07	0.02	0.52	4.90	0.35

913
 914
 915
 916

Supplementary Table 4. The r-PLS values of PLS1 (above diagonal) and p-values (below diagonal) of each 2BPLS analysis. Significant values are in bold.

	Dentary	Compound	Quadrate	Supratemporal	Pterygoid	Ectopterygoid	Palatine	Maxilla
Dentary		0.634	0.619	0.665	0.476	0.822	0.651	0.711
Compound	0.009		0.589	0.465	0.407	0.573	0.561	0.578
Quadrate	0.043	0.053		0.674	0.647	0.686	0.651	0.65
Supratemporal	0.029	0.49	0.013		0.560	0.73	0.692	0.686
Pterygoid	0.158	0.312	0.022	0.111		0.453	0.74	0.606
Ectopterygoid	0.001	0.043	0.028	0.012	0.197		0.611	0.806
Palatine	0.051	0.123	0.051	0.02	0.003	0.105		0.747
Maxilla	0.009	0.115	0.045	0.041	0.087	0.001	0.003	

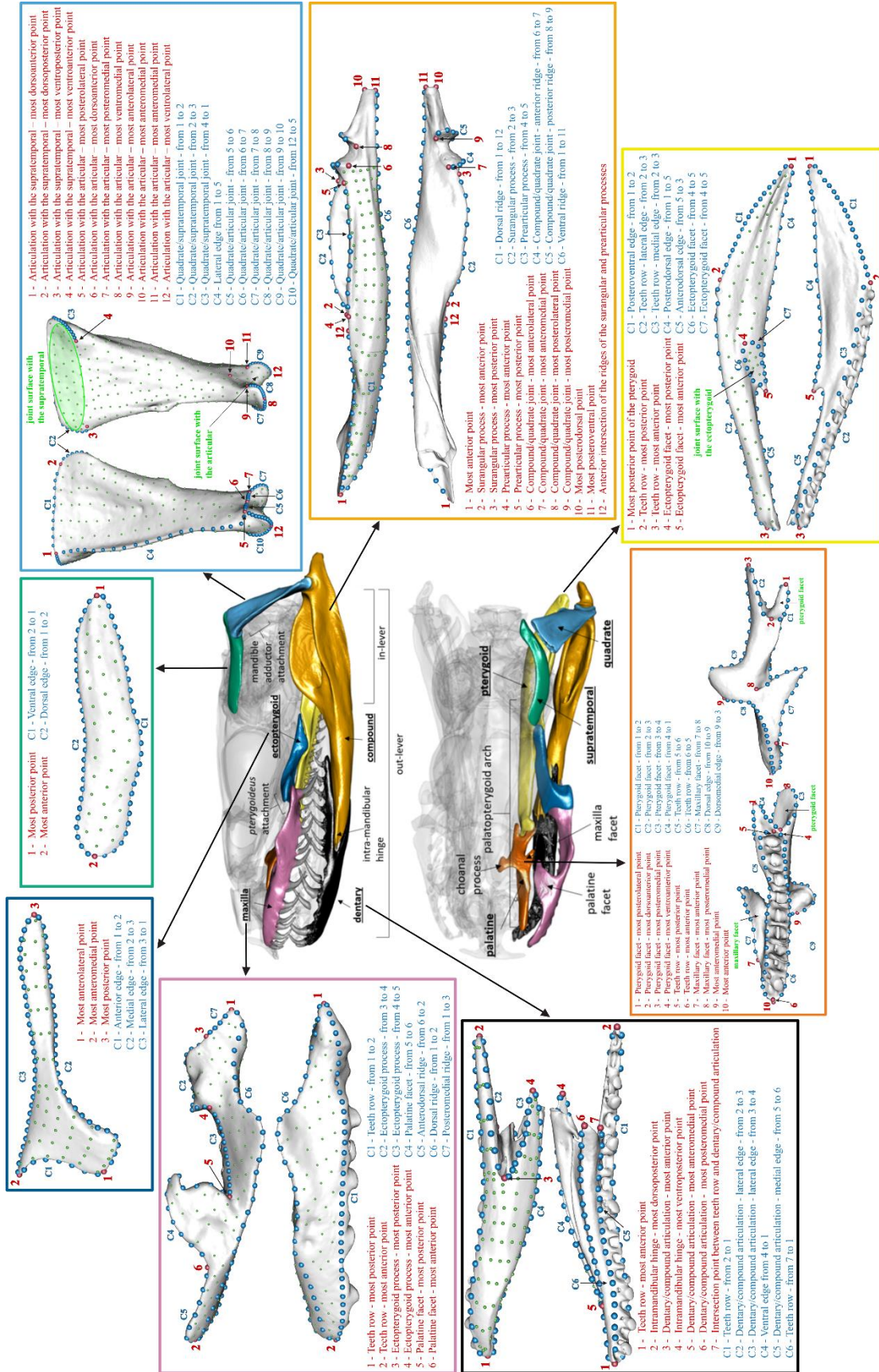
917
 918
 919

Supplementary Table 5. The z-PLS values of PLS1 (above diagonal) and p-values (below diagonal) of each 2BPLS analysis. Significant values are in bold.

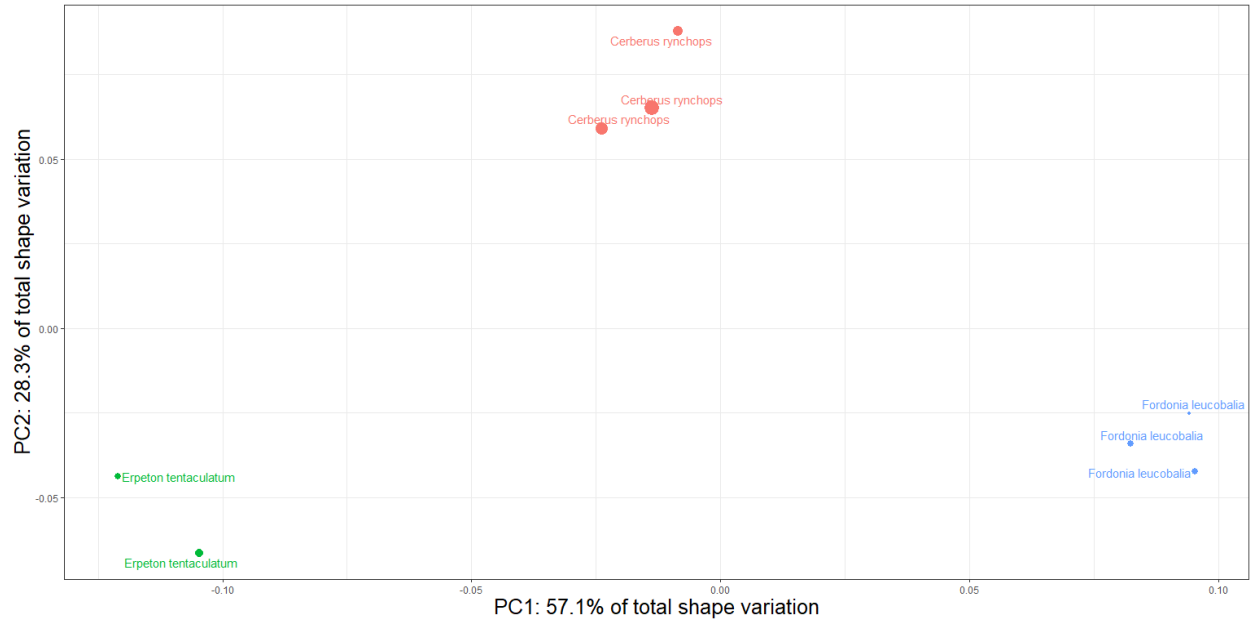
	Dentary	Compound	Quadrate	Supratemporal	Pterygoid	Ectopterygoid	Palatine	Maxilla
Dentary		2.905	1.910	1.980	1.035	4.058	1.818	2.435
Compound	0.009		1.827	0	0.389	2.073	1.192	1.262
Quadrate	0.043	0.053		2.362	2.342	2.348	1.852	1.874
Supratemporal	0.029	0.49	0.013		1.255	2.512	2.138	1.766
Pterygoid	0.158	0.312	0.022	0.111		0.8233	3.040	1.452
Ectopterygoid	0.001	0.043	0.028	0.012	0.197		1.4378	3.272
Palatine	0.051	0.123	0.051	0.02	0.003	0.105		2.944
Maxilla	0.009	0.115	0.045	0.041	0.087	0.001	0.003	

920 Supplementary Table 6. Alternative hypotheses of modularity and their support, measured as phylogenetic-corrected
 921 Z_{CR} , for both common and local superimposition procedures. The lower the Z_{CR} and CR values, the stronger the
 922 modular signal. ‘Else’ refers to all the other bones not yet mentioned as part of their own module. Rows are ordered
 923 by Z_{CR} of common superimposition and are colored according to strength of modular signal.

#	Hypothesis	Modules	Common Superimposition		Local Superimpositions	
			CR	Z_{CR}	CR	Z_{CR}
1	[dentary, compound] + [else]	2	0.63	-31.18	0.65	-27.02
2	[dentary, compound, quadrate, supratemporal] + [pterygoid, palatine, ectopterygoid, maxilla]	2	0.76	-31.03	0.77	-26.08
15	[dentary, compound] + [quadrate, supratemporal] + [pterygoid, palatine, ectopterygoid] + [maxilla]	4	0.72	-30.93	0.62	-28.13
9	[dentary, compound] + [quadrate, supratemporal] + [pterygoid, palatine, ectopterygoid, maxilla]	3	0.76	-30.86	0.74	-25.52
16	[dentary, compound] + [quadrate, supratemporal] + [pterygoid, palatine] + [maxilla, ectopterygoid]	4	0.76	-30.75	0.76	-24.79
10	[dentary, compound, quadrate, supratemporal] + [maxilla] + [pterygoid, palatine, ectopterygoid]	3	0.74	-30.68	0.58	-28.12
17	[dentary, anterior compound] + [posterior compound, quadrate, supratemporal] + [pterygoid, palatine] + [ectopterygoid, maxilla]	4	0.77	-30.61	0.76	-24.50
4	[dentary, compound, quadrate, maxilla] + [supratemporal, pterygoid, palatine, ectopterygoid]	2	0.82	-30.54	0.68	-28.14
12	[dentary, maxilla] + [compound, quadrate, supratemporal] + [pterygoid, palatine, ectopterygoid]	3	0.81	-30.53	0.73	-26.69
14	[dentary, anterior compound] + [posterior compound, quadrate, supratemporal] + [pterygoid, palatine, ectopterygoid, maxilla]	3	0.78	-30.47	0.77	-24.24
19	Complete modularity except [pterygoid, palatine]	7	0.71	-30.37	0.65	-24.35
21	Complete modularity	8	0.73	-30.21	0.67	-24.72
11	[dentary, compound, quadrate, supratemporal] + [maxilla, ectopterygoid] + [pterygoid, palatine]	3	0.81	-30.15	0.81	-21.25
5	[dentary, anterior compound] + [else]	2	0.74	-30.11	0.74	-22.45
18	Complete modularity except [pterygoid, palatine] + [dentary, compound]	6	0.75	-29.78	0.68	-23.66
20	Complete modularity except [dentary, compound]	7	0.77	-29.42	0.72	-22.47
3	[maxilla, ectopterygoid] + [else]	2	0.85	-29.13	0.85	-18.27
8	[posterior compound, quadrate, supratemporal] + [else]	2	0.90	-28.12	0.98	-3.57
6	[pterygoid, palatine] + [else]	2	0.90	-25.91	0.83	-17.53
13	[dentary, compound, maxilla, ectopterygoid] + [quadrate, supratemporal] + [pterygoid, palatine]	3	0.92	-25.26	0.86	-18.04
7	[quadrate, supratemporal] + [else]	2	0.98	-12.00	0.98	-3.36



Supplemental Figure 1. The bones analyzed in this paper (middle two skulls) and their respective landmark configurations. Red indicates anatomical landmarks, blue curve semi-landmarks and green surface semi-landmarks, along with a list of description of each landmark (red) and curves (blue) and some important anatomical features (green).



925

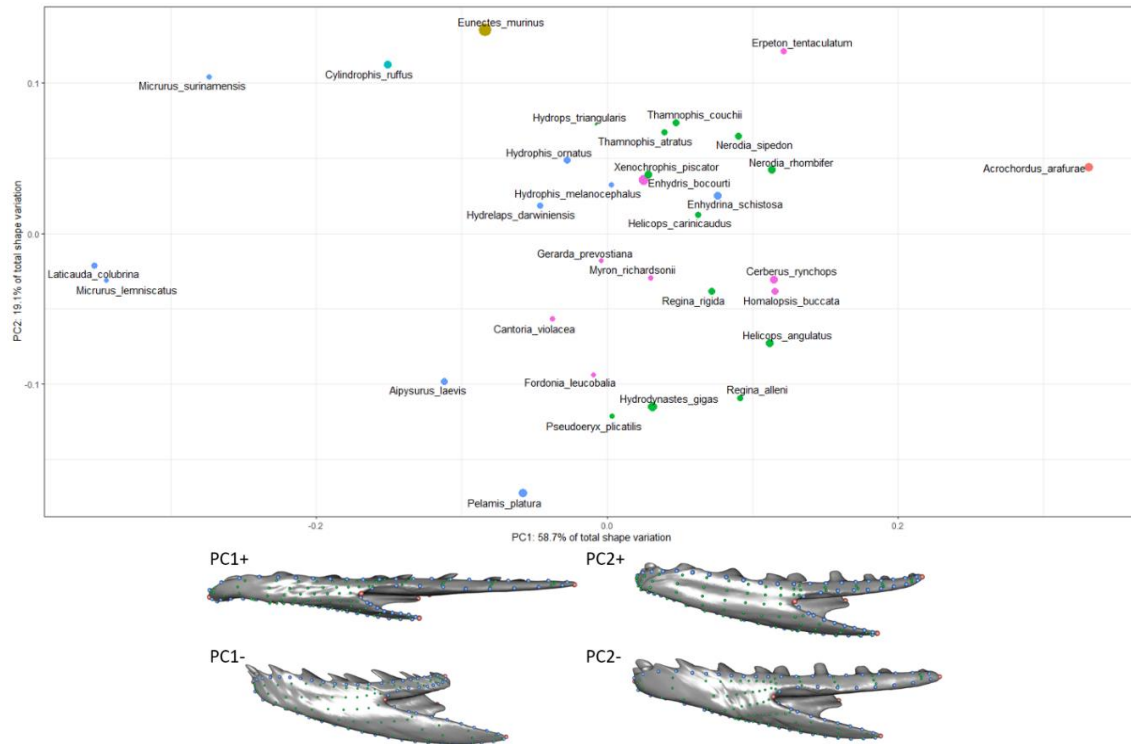
926

927

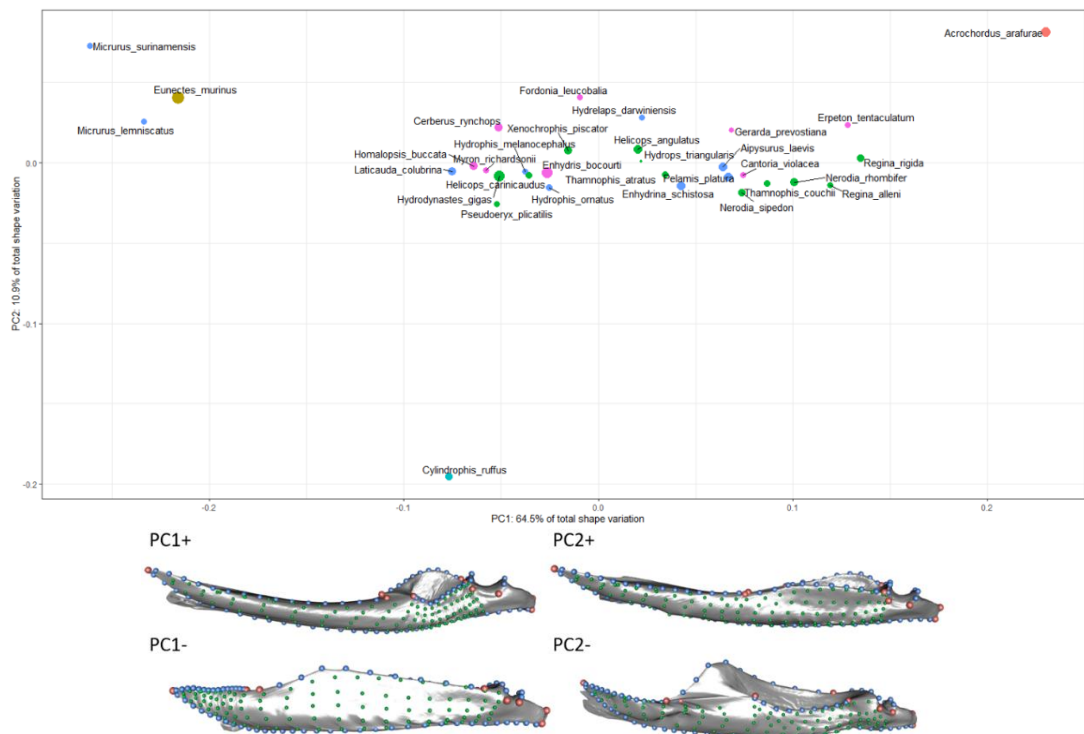
928

929

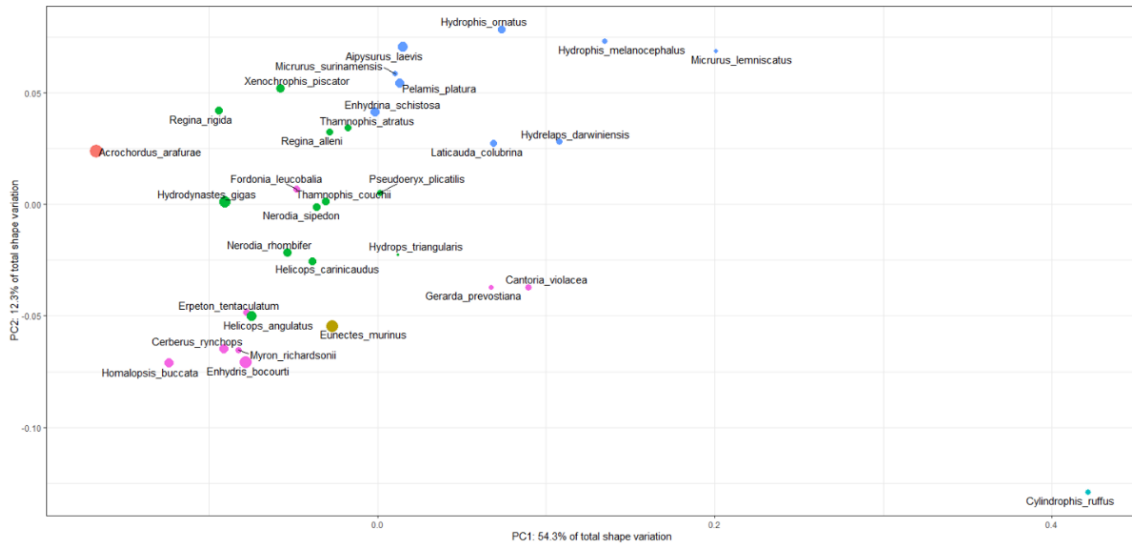
Supplemental Figure 2. Principal component morphospace from a common superimposition (GPA_{All}) of individual specimens of three homalopsid snakes: *Erpeton tentaculatum* (green), *Fordonia leucobalia* (blue), and *Cerberus rynchops* (orange). Note that individual specimens of each species group together much more closely than different species.



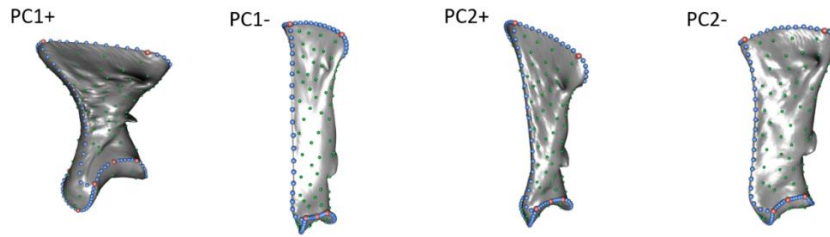
931
932
933
934
935
936
Supplementary Figure 3. Morphospace of the first two principal components of the dentary (above), and axes of shape variation along the first two principal components in lateral view (below). Size of each point (species) corresponds to centroid size of the dentary and color corresponds to taxonomic family as in Figure 1. This scheme is consistent for Supplementary figures 3-10.



941



942



943

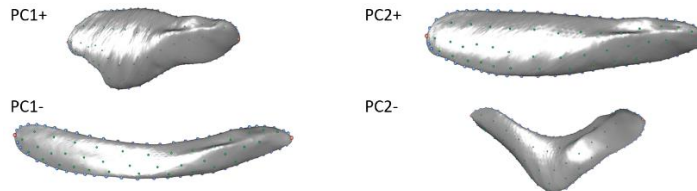
944

945

946

Supplementary Figure 5. Morphospace of the first two principal components of the quadrate (above), and axes of shape variation along the first two principal components in lateral view (below).

947



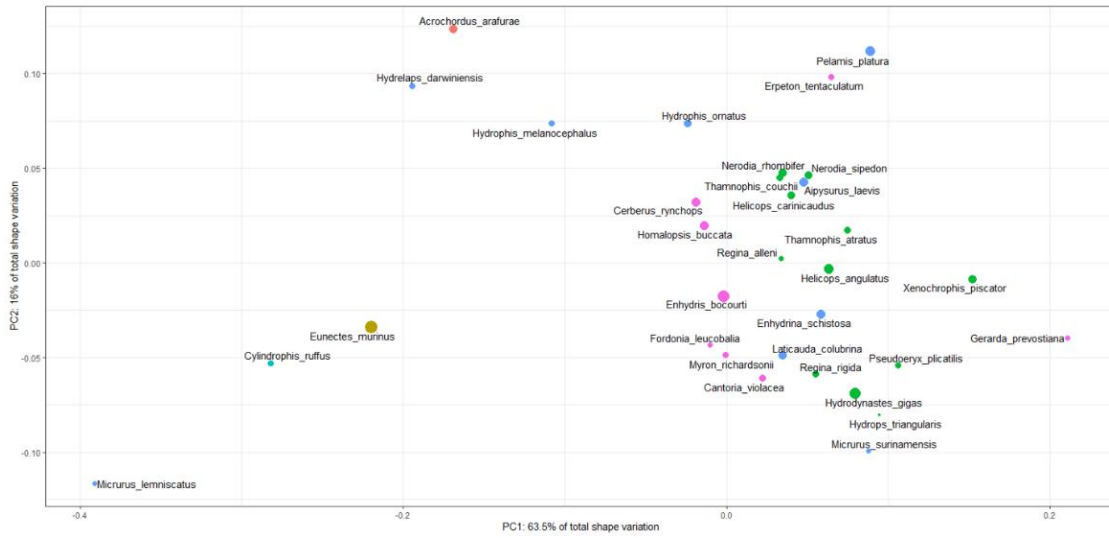
948

949

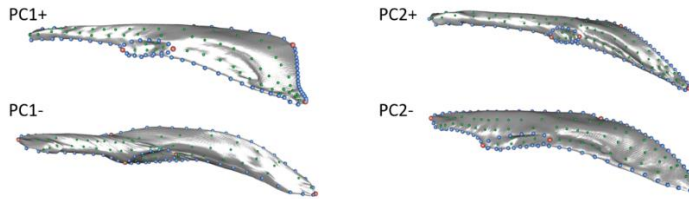
950

Supplementary Figure 6. Morphospace of the first two principal components of the supratemporal (above), and axes of shape variation along the first two principal components in lateral view (below).

951



952



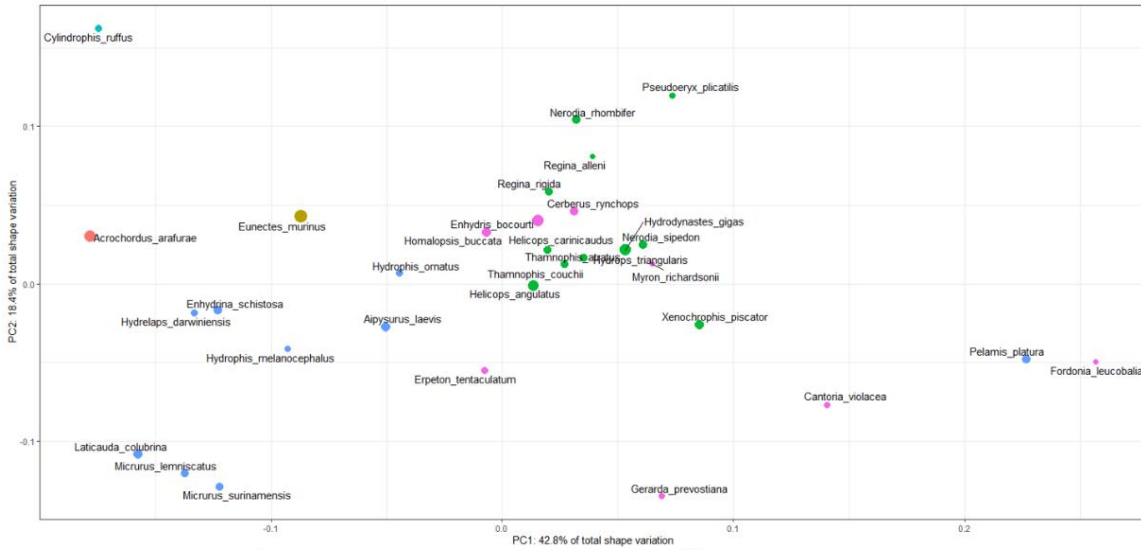
953

954

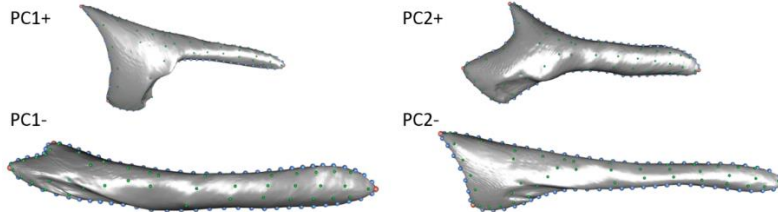
955

956

Supplementary Figure 7. Morphospace of the first two principal components of the pterygoid (above), and axes of shape variation along the first two principal components in dorsal view (below).



957



958

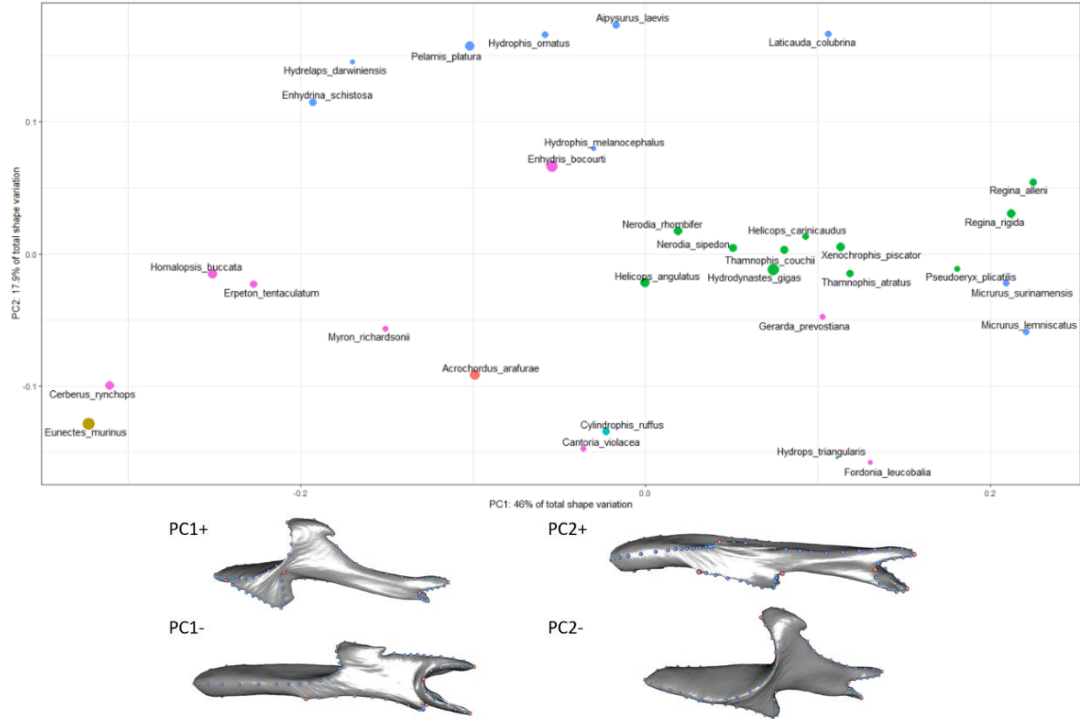
959

960

961

Supplementary Figure 8. Morphospace of the first two principal components of the ectopterygoid (above), and axes of shape variation along the first two principal components in dorsal view (below).

962



963

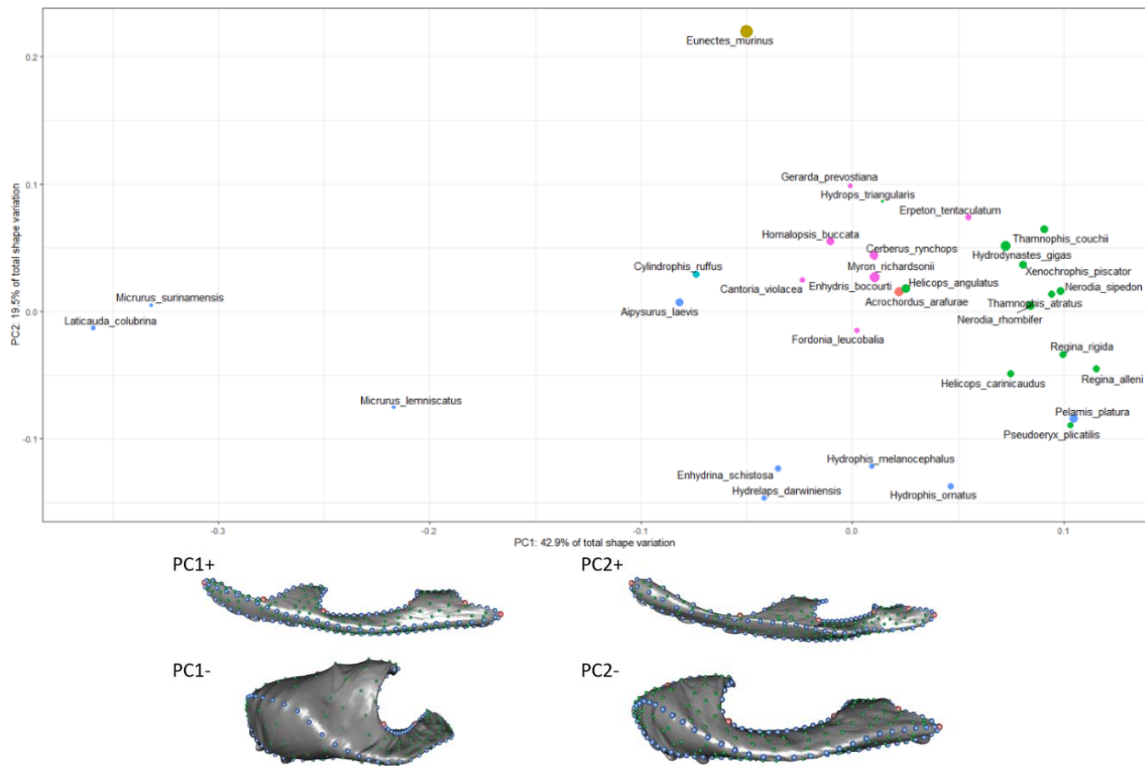
964

965

966

Supplementary Figure 9. Morphospace of the first two principal components of the palatine (above), and axes of shape variation along the first two principal components in dorsal view (below).

967

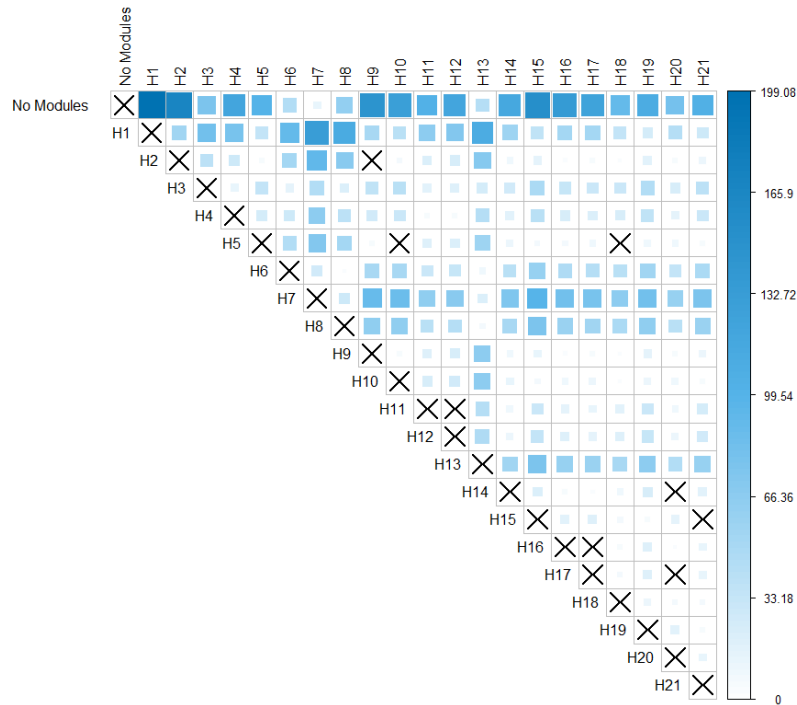


968

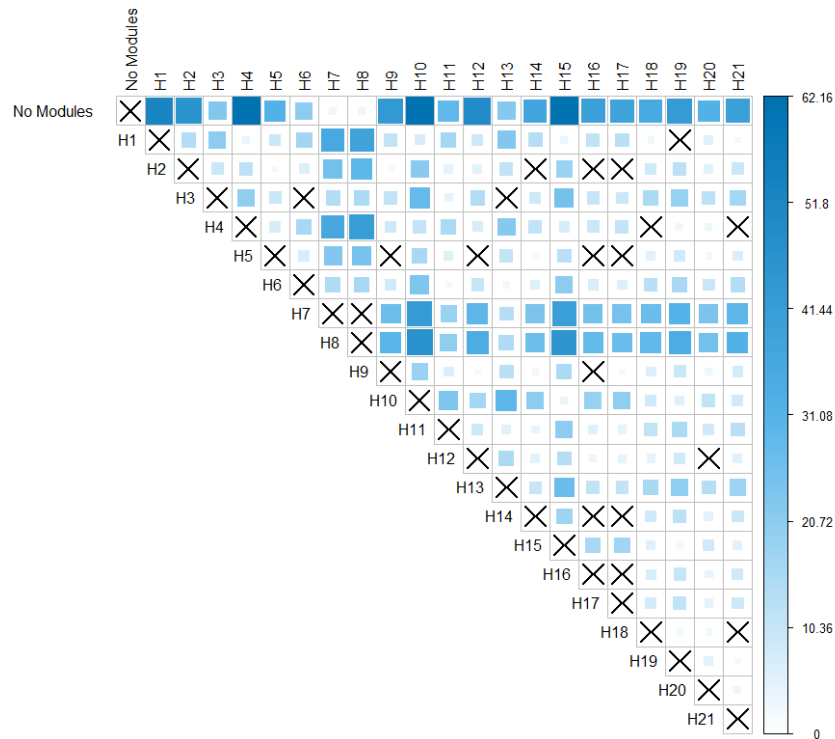
969

970

Supplementary Figure 10. Morphospace of the first two principal components of the maxilla (above), and axes of shape variation along the first two principal components in dorsal view (below).



971
972 Supplementary Figure 11. Pairwise effect sizes of alternative hypotheses of modularity of the common
973 superimposition. Darker blue cells correspond to higher effect sizes and larger differences between strength of modular
974 signal between alternative hypotheses. Insignificant (i.e., not significantly different support) values are marked by
975 'X's. 'No Modules' refers to the null hypothesis of complete integration.
976



977
978 Supplementary Figure 12. Pairwise effect sizes of alternative hypotheses of modularity of the local superimposition
979 dataset. Darker blue cells correspond to higher effect sizes and larger differences between strength of modular signal
980 between alternative hypotheses. Insignificant (i.e., not significantly different support) values are marked by 'X's. 'No
981 Modules' refers to the null hypothesis of complete integration.